Supporting Information

for

High-Spin Iron (II) Alkynyl Complexes with *N*-Heterocyclic Carbene Ligation: Synthesis, Characterization, and Reactivity Study

Xiaojie Wang, Jia Zhang, Lei Wang, and Liang Deng*

State Key Laboratory of Organometallic Chemistry, Shanghai Institute of Organic Chemistry, Chinese Academy of Sciences, 345 Lingling Road, Shanghai, P. R. China, 200032

deng@sioc.ac.cn

Table of Contents

Table S1. Crystal data and summary of data collection and refinement for **1**, and **3**-**5**.[a,b]

	1	**3**	**4**	**5**
Temperature, K	143(2)	140(2)	140(2)	140(2)
formula	$C_{34}H_{58}FeN_4$	$C_{36}H_{61}FeN_5Si$	$C_{24}H_{54}FeP_4$	$C_{43}H_{74}FeN_6$
fw	578.69	647.83	522.40	730.93
crystal system	Hexagonal	Orthorhombic	Monoclinic	Monoclinic
space group	*R*3	*P*bca	$P2_1/c$	$P2_1/c$
a, Å	27.826(3)	18.8526(14)	15.0186(14)	22.574(2)
b, Å	27.826(3)	19.5760(15)	10.5172(10)	9.7981(9)
c, Å	13.4682(14)	20.9753(16)	20.224(19)	20.4582(18)
α, deg	90	90	90	90
β, deg	90	90	105.155(2)	96.290(2)
γ, deg	120	90	90	90
V, Å^3	9030.9(17)	7741.1(10)	3083.5(5)	4497.8(7)
Z	9	8	4	4
d_{calcd}, g/cm^3	0.958	1.112	1.125	1.079
2*θ* range, deg	3.46 to 61.02	3.57-61.09	2.80-61.16	1.81-61.06
GOF (F^2)	1.023	1.017	1.032	1.024
R1[b]	0.0563,[d] 0.0799[e]	0.0520,[d] 0.0974[e]	0.0360,[d] 0.0543[e]	0.0428,[d] 0.0684[e]
*w*R2[c]	0.1294,[d] 0.1386[e]	0.1322,[d] 0.1618[e]	0.0951,[d] 0.1073[e]	0.1098,[d] 0.1240[e]

[a] Collected using Mo Kα radiation (λ = 0.71073 Å). [b] $R1 = \Sigma[(F_o - F_c)] / \Sigma(F_o)$. [c] $wR2 = \{\Sigma[w(F_o^2 - F_c^2)^2 / \Sigma[w(F_o^2)^2]]^{½}$. [d] $I > 2\sigma(I)$. [e] All data.

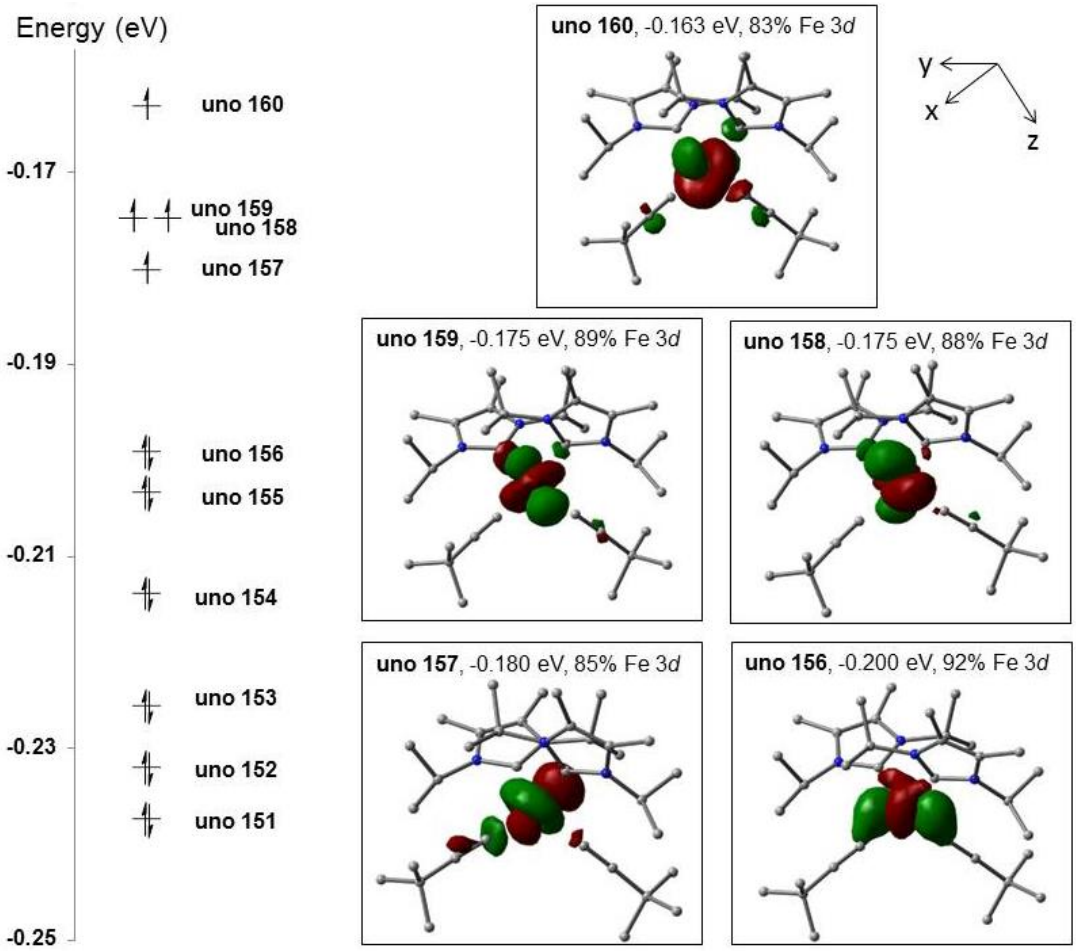

Figure S1. Frontier UNO energy level diagram for $(IPr_2Me_2)_2Fe(C{\equiv}CBu^t)_2$ (S = 2) and selected UNO plots.

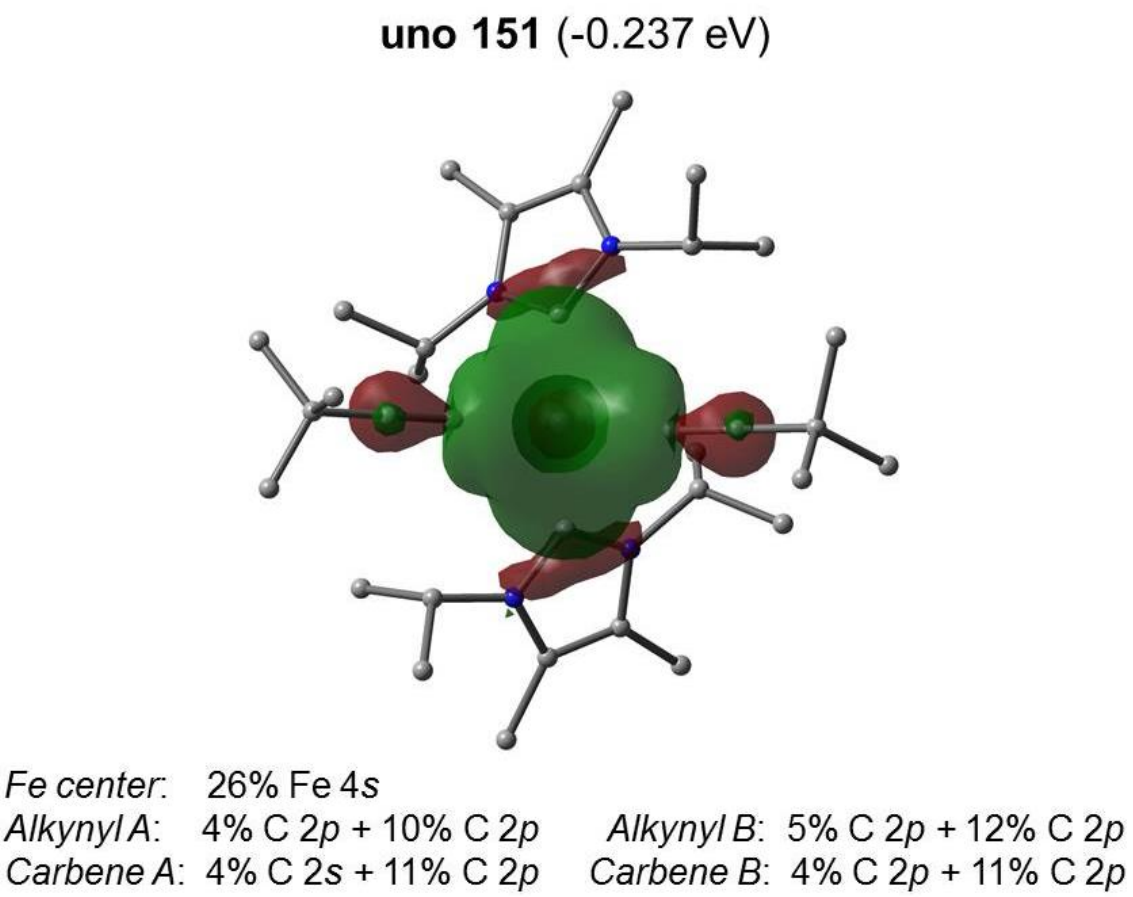

Figure S2. The UHF natural orbital 151 of $(IPr_2Me_2)_2Fe(C{\equiv}CBu^t)_2$ (S = 2), depicted using isodensity at 0.03 au.

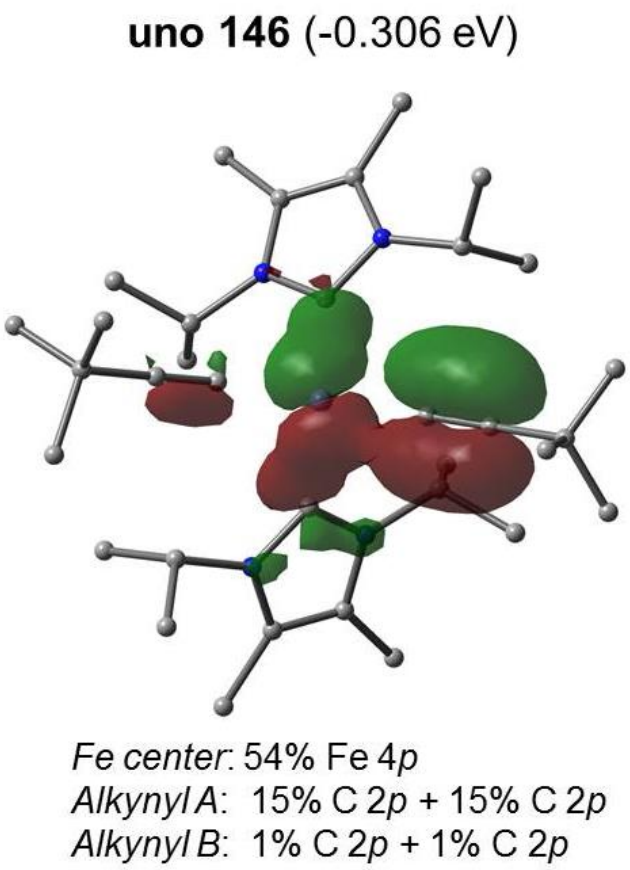

Figure S3. The UHF natural orbital 146 of $(IPr_2Me_2)_2Fe(C{\equiv}CBu^t)_2$ (S = 2), depicted using isodensity at 0.03 au.

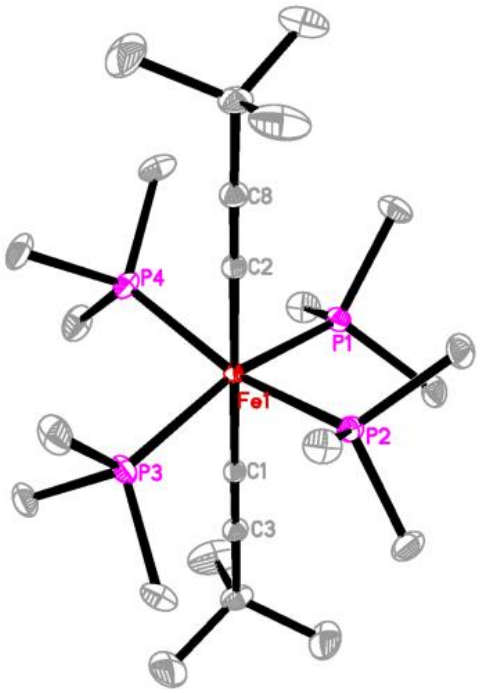

Figure S4. Molecular structure of 4, showing 30% probability ellipsoilds and the partial atom numbering scheme. Selected bond distances (Å) and angles (deg): Fe(1)-C(1) 1.9495(16), Fe(1)-C(2) 1.9420(16), Fe(1)-P(1) 2.2197(5), Fe(1)-P(2) 2.2274(5), Fe(1)-P(3) 2.2320(5), Fe(1)-P(4) 2.2262(5). C(1)-C(3) 1.222(2), C(2)-C(8) 1.223(2).

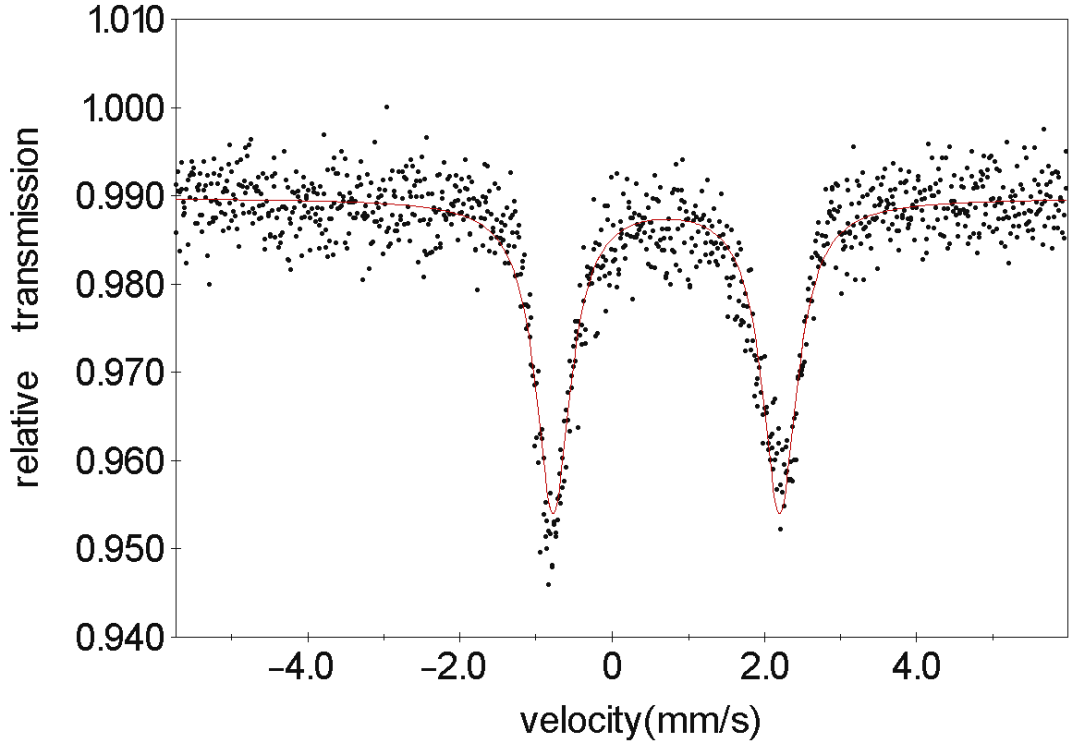

Figure S5. The zero-field ^{57}Fe Mössbauer spectrum of $(IPr_2Me_2)_2FeI_2$ recorded at 80 K.

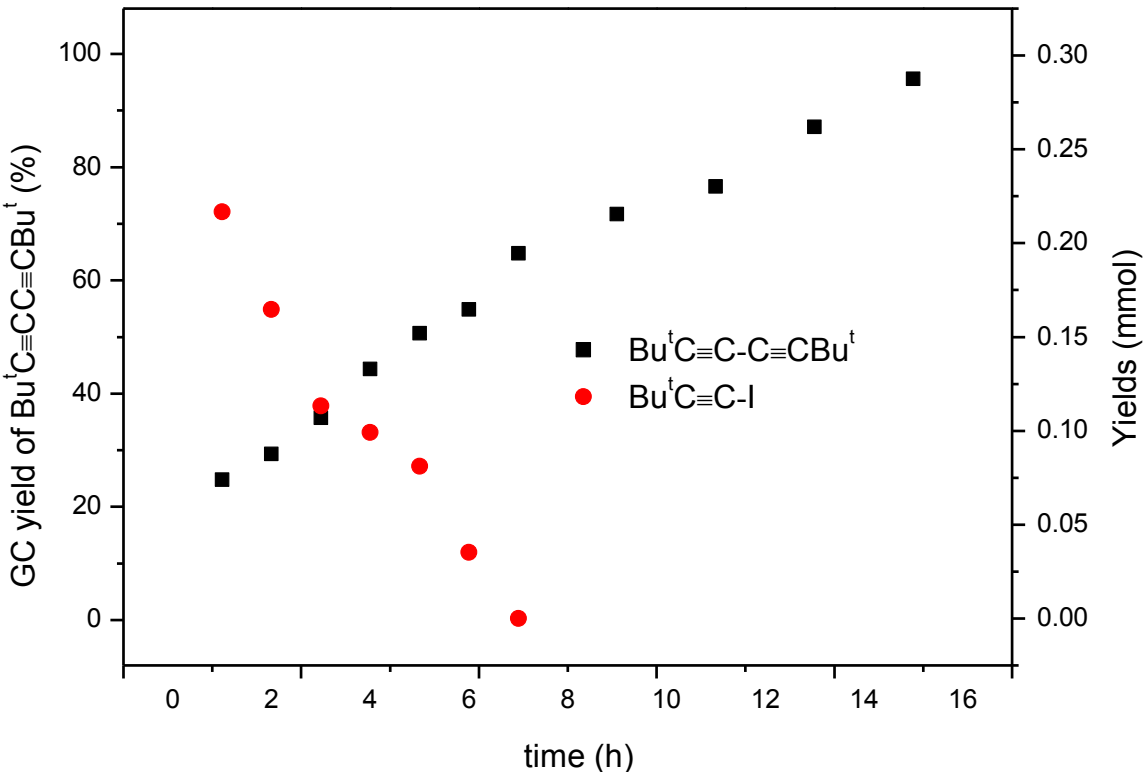

Figure S6. GC-Yields of organic products versus time for the reaction of 1 (0.30 mmol) with I_2 (0.30 mmol) in THF (2 mL).

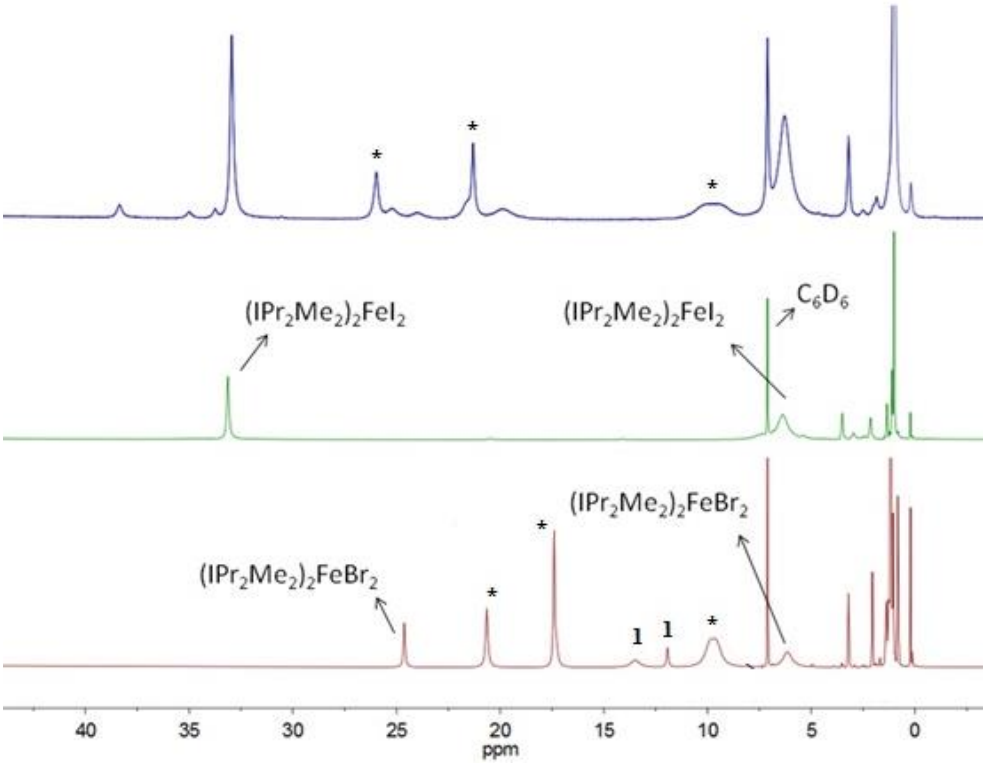

Figure S7. ^{1}H NMR spectra of the reaction of 1 (0.04 mmol) with I_2 (1 equiv.) in C_6D_6 (0.4 mL) after 10 min (upper), after 6 h (middle), and the reaction of 1 (0.04 mmol) with *n*-$C_8H_{17}Br$ (1 equiv.) in C_6D_6 (0.4 mL) after 43 h (bottom). Peaks labeled with stars are signals of the intermediates, presumably $(IPr_2Me_2)_2Fe(C{\equiv}CBu^t)X$ (X = I or Br).

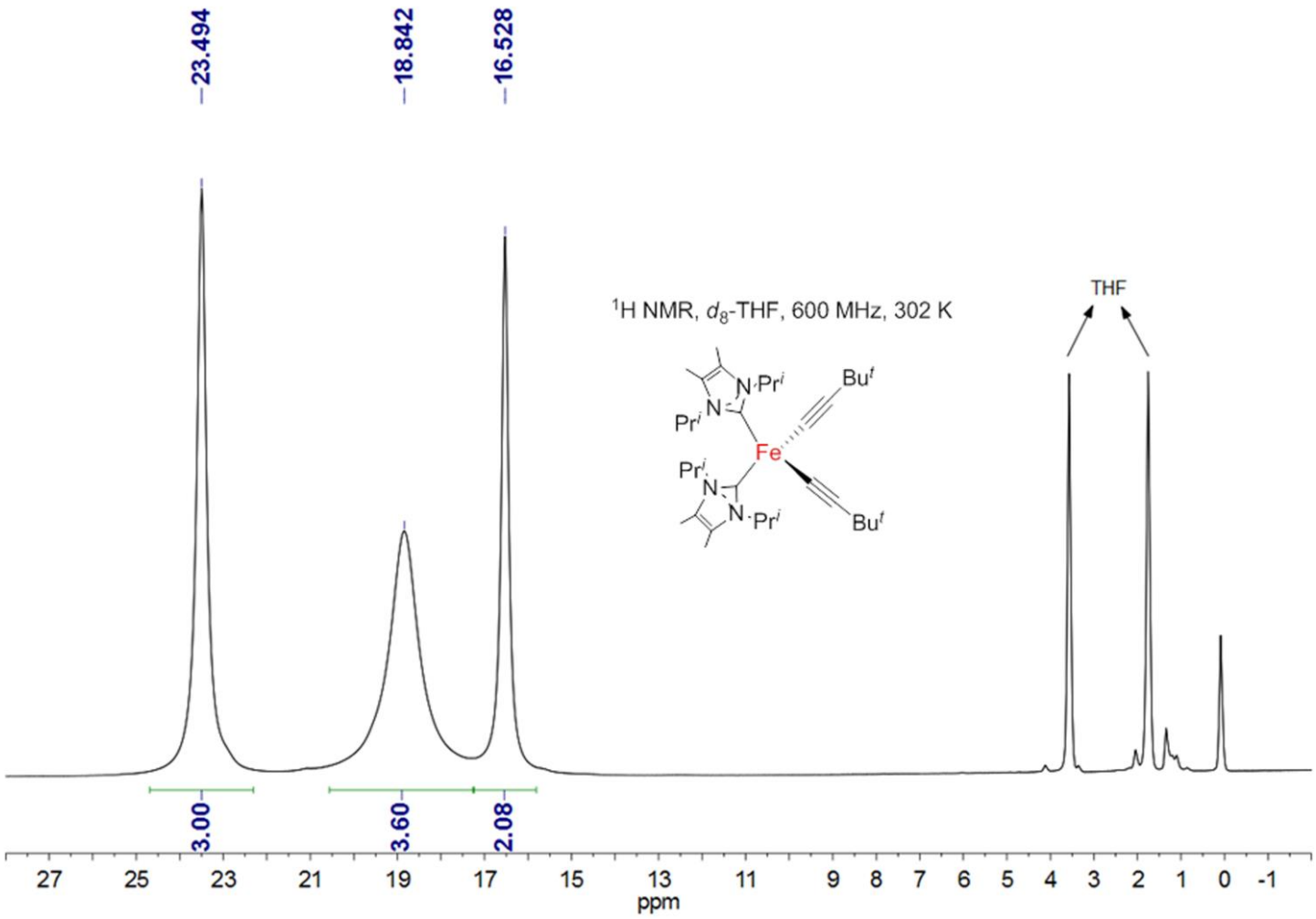

Figure S8. ^{1}H NMR spectrum of [$(IPr_2Me_2)_2Fe(C{\equiv}CBu^t)_2$] (**1**) in THF-$d_8$.

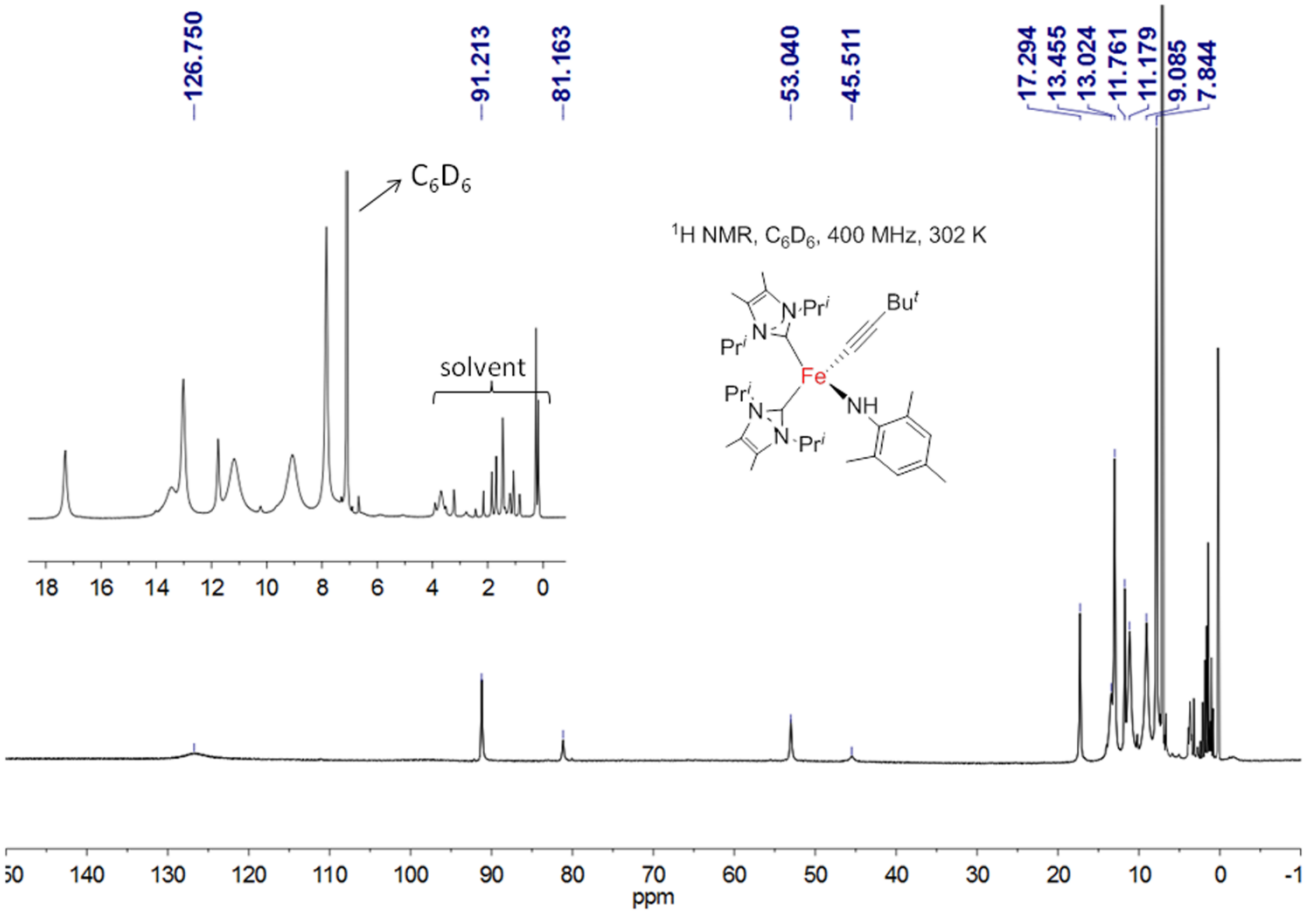

Figure S9. ^{1}H NMR spectrum of [$(IPr_2Me_2)_2Fe(C{\equiv}CBu^t)(NHMes)$] (**2**) in C_6D_6.

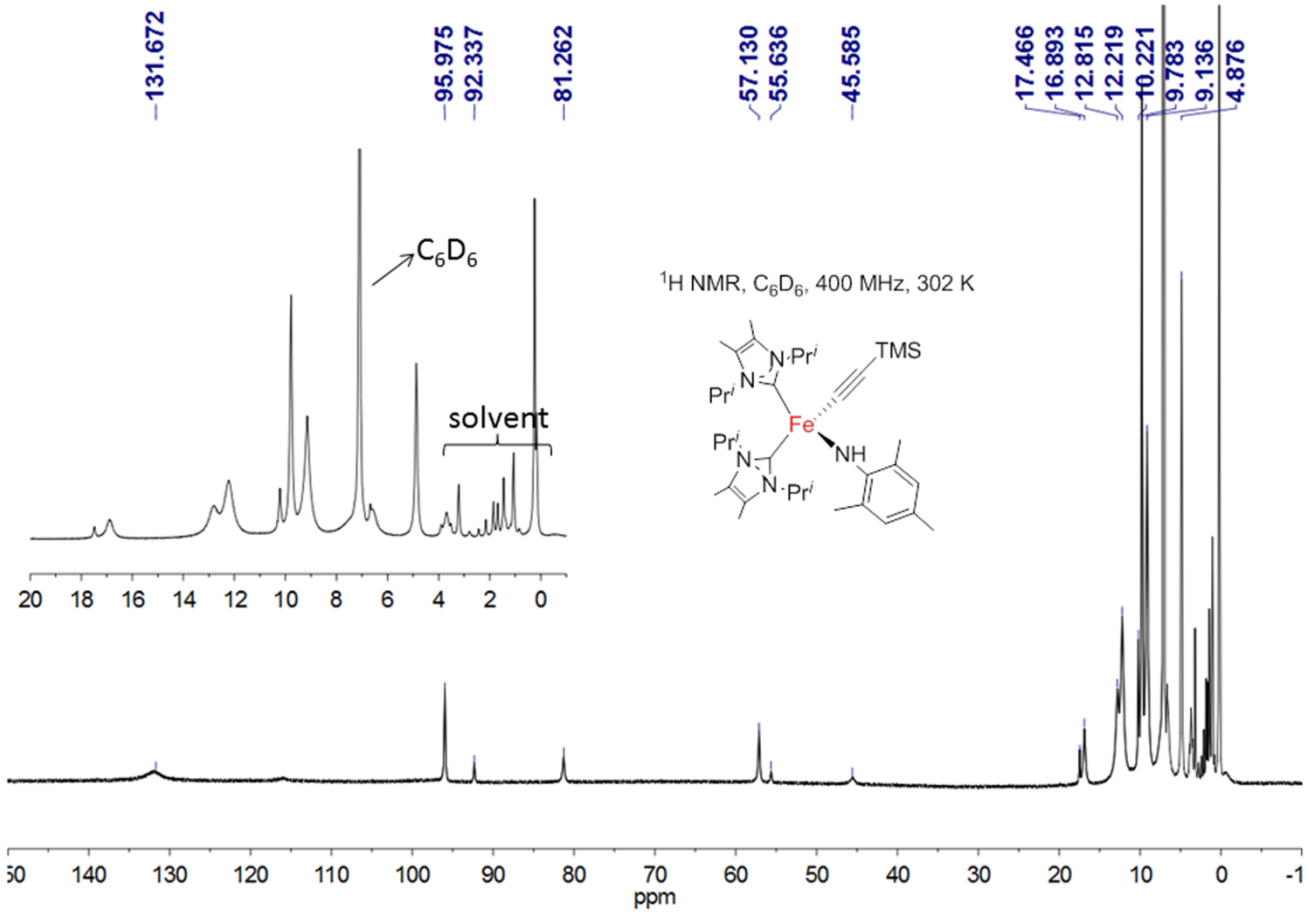

Figure S10. ^{1}H NMR spectrum of [(IPr$_2$Me$_2$)$_2$Fe(C≡CTMS)(NHMes)] (**3**) in C_6D_6.

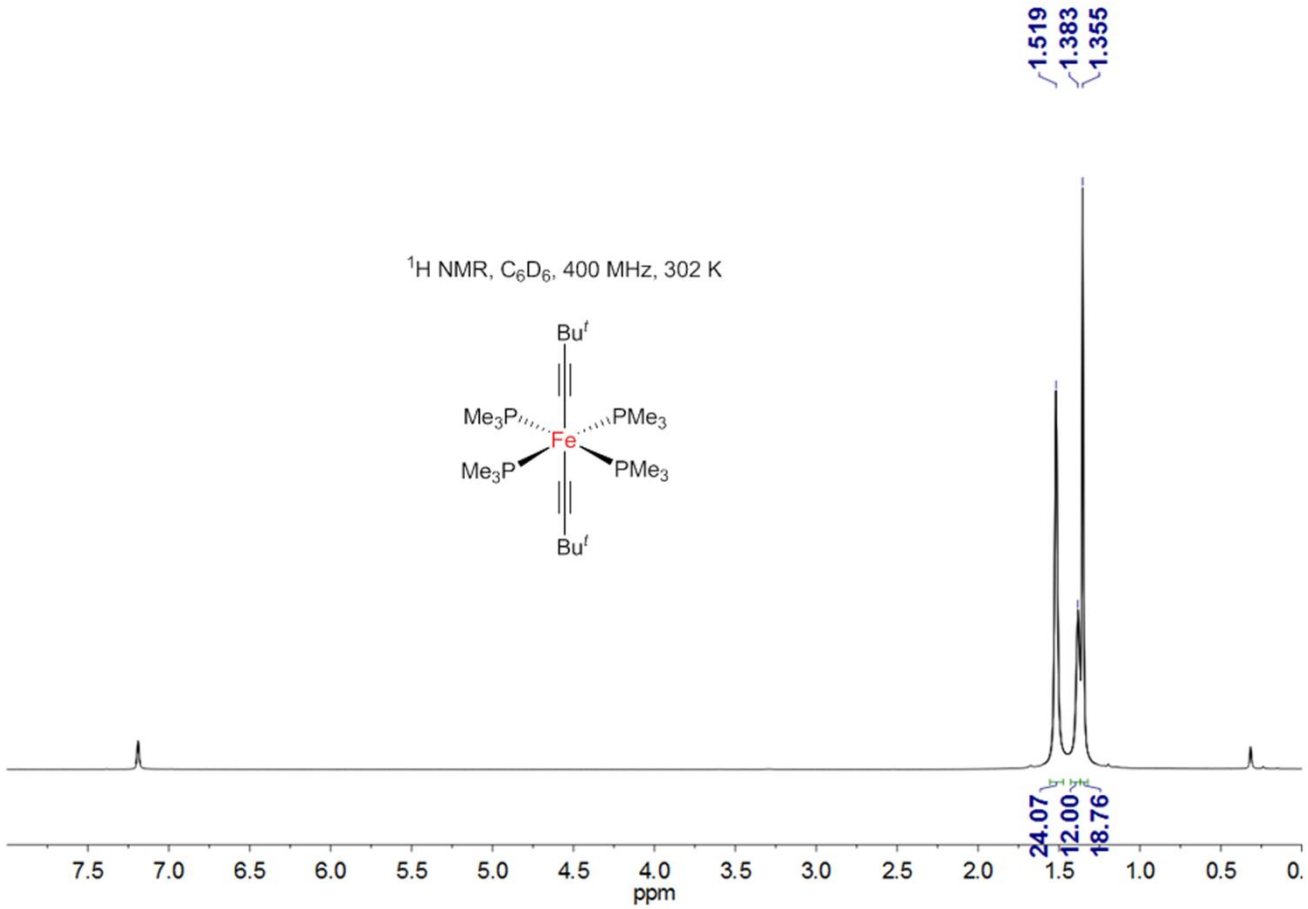

Figure S11. ^{1}H NMR spectrum of $[(PMe_3)_4Fe(C{\equiv}CBu^t)_2]$ (**4**) in C_6D_6.

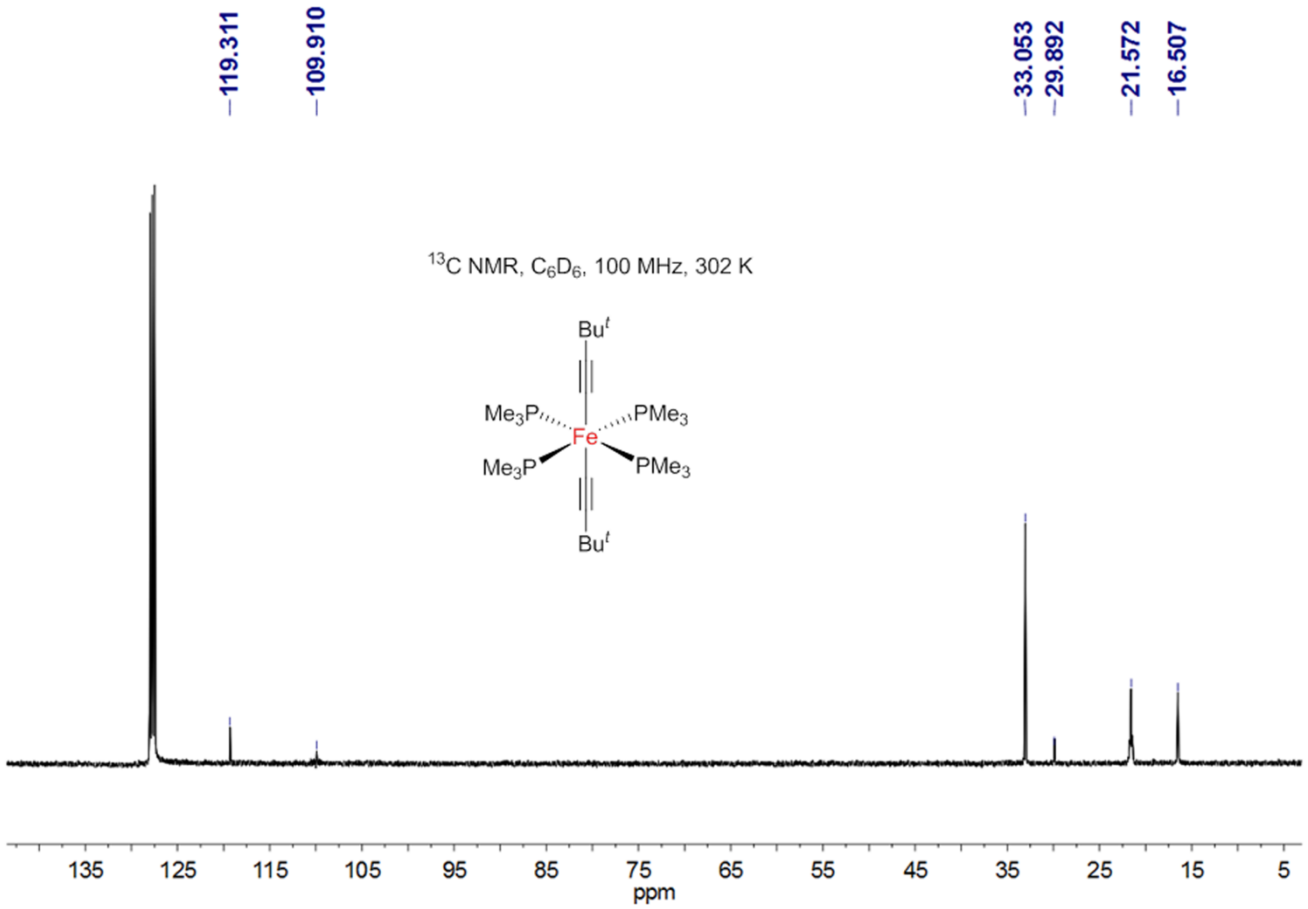

Figure S12. ^{13}C NMR spectrum of $[(PMe_3)_4Fe(C{\equiv}CBu^t)_2]$ (**4**) in C_6D_6.

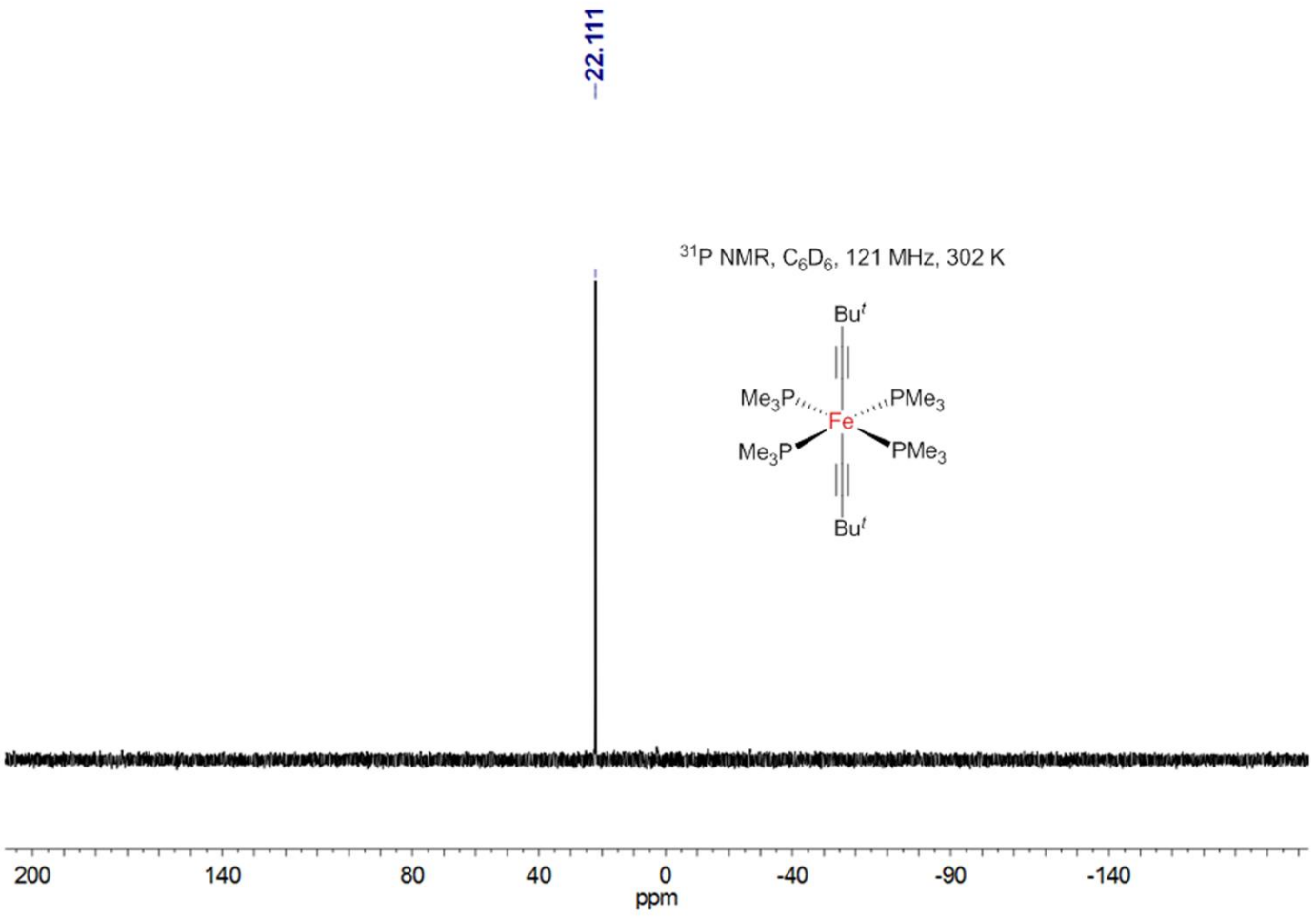

Figure S13. ^{31}P NMR spectrum of $[(PMe_3)_4Fe(C{\equiv}CBu^t)_2]$ (**4**) in C_6D_6.

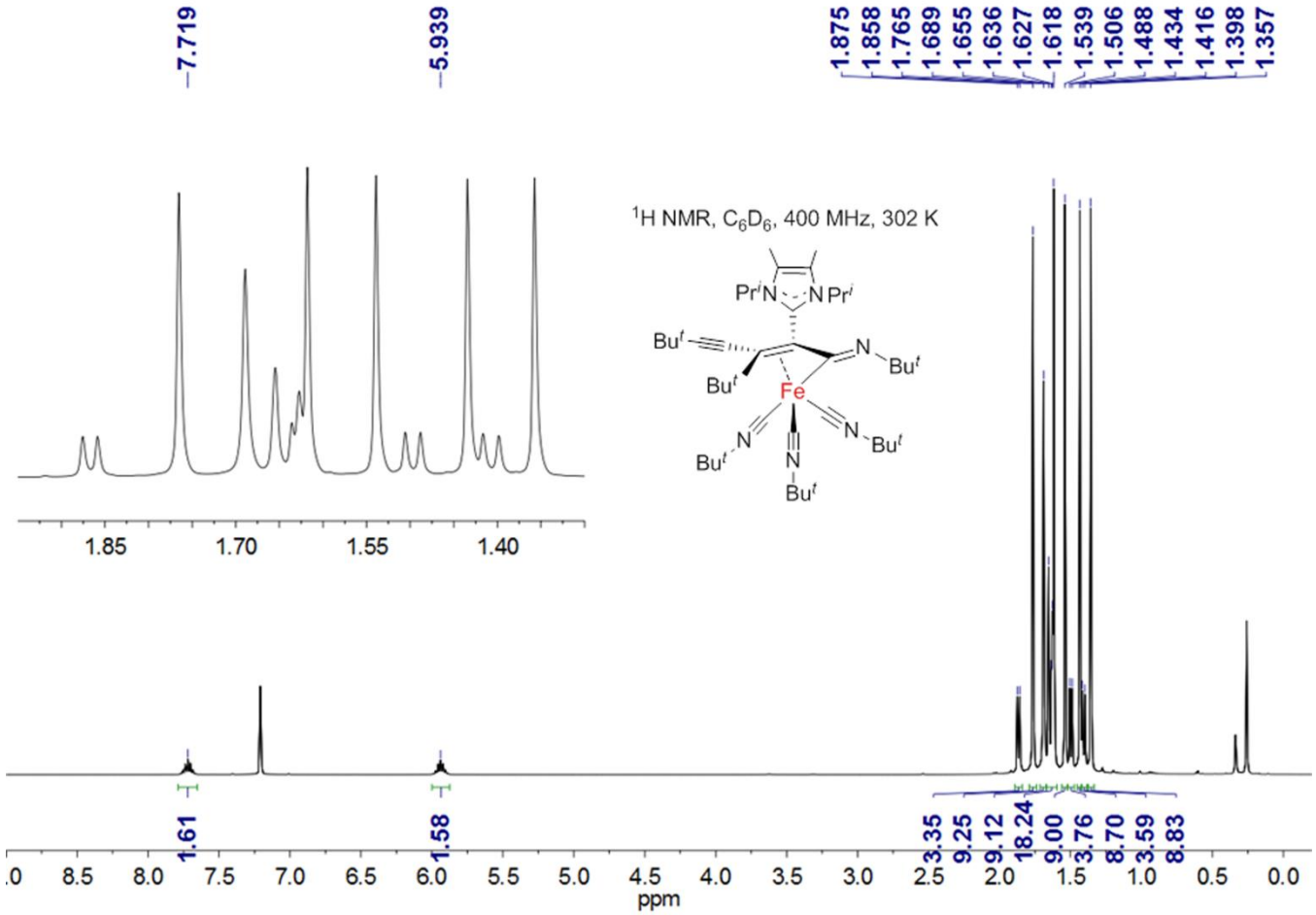

Figure S14. ^{1}H NMR spectrum of **5** in C_6D_6.

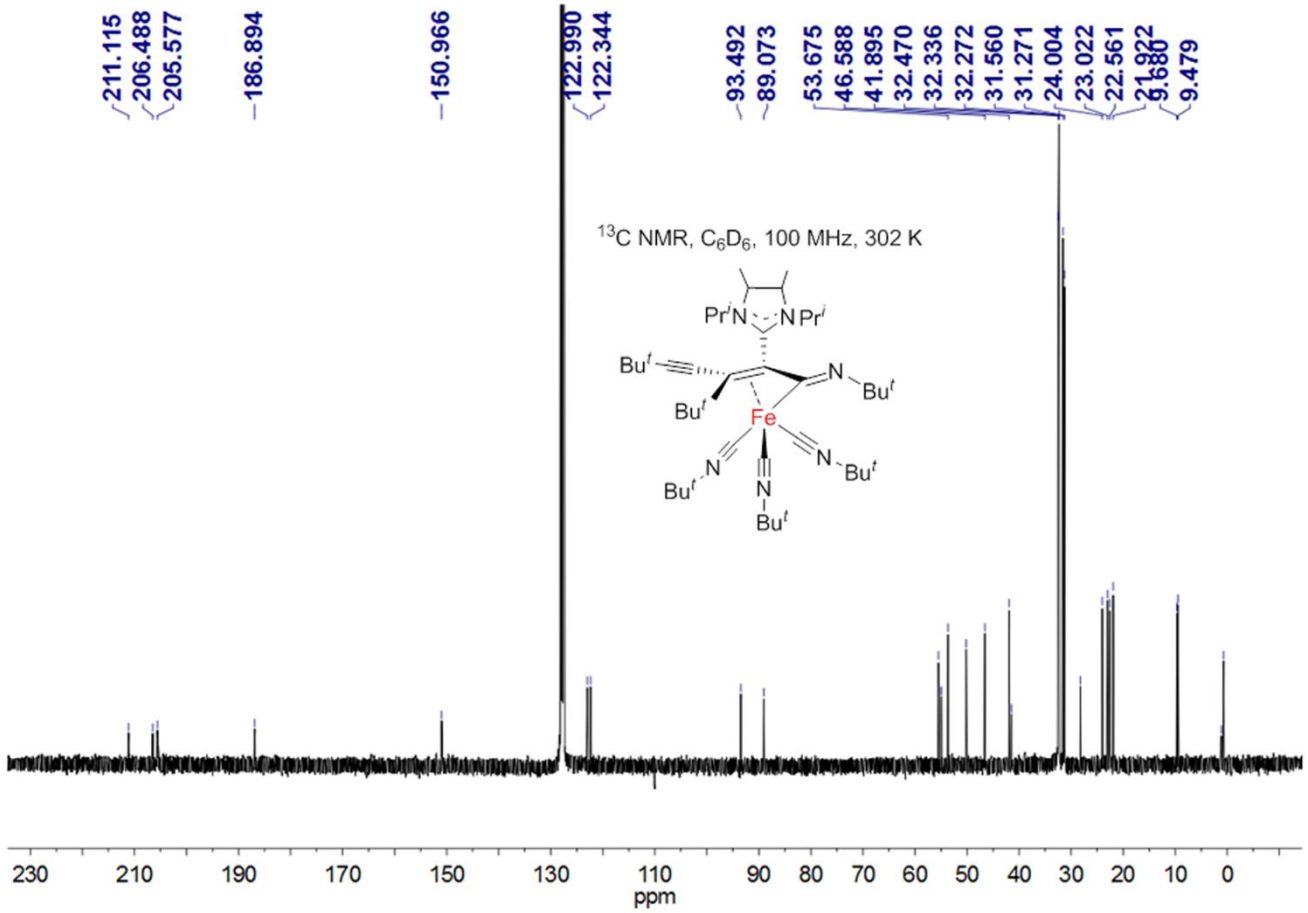

Figure S15. ^{13}C NMR spectrum of **5** in C_6D_6.

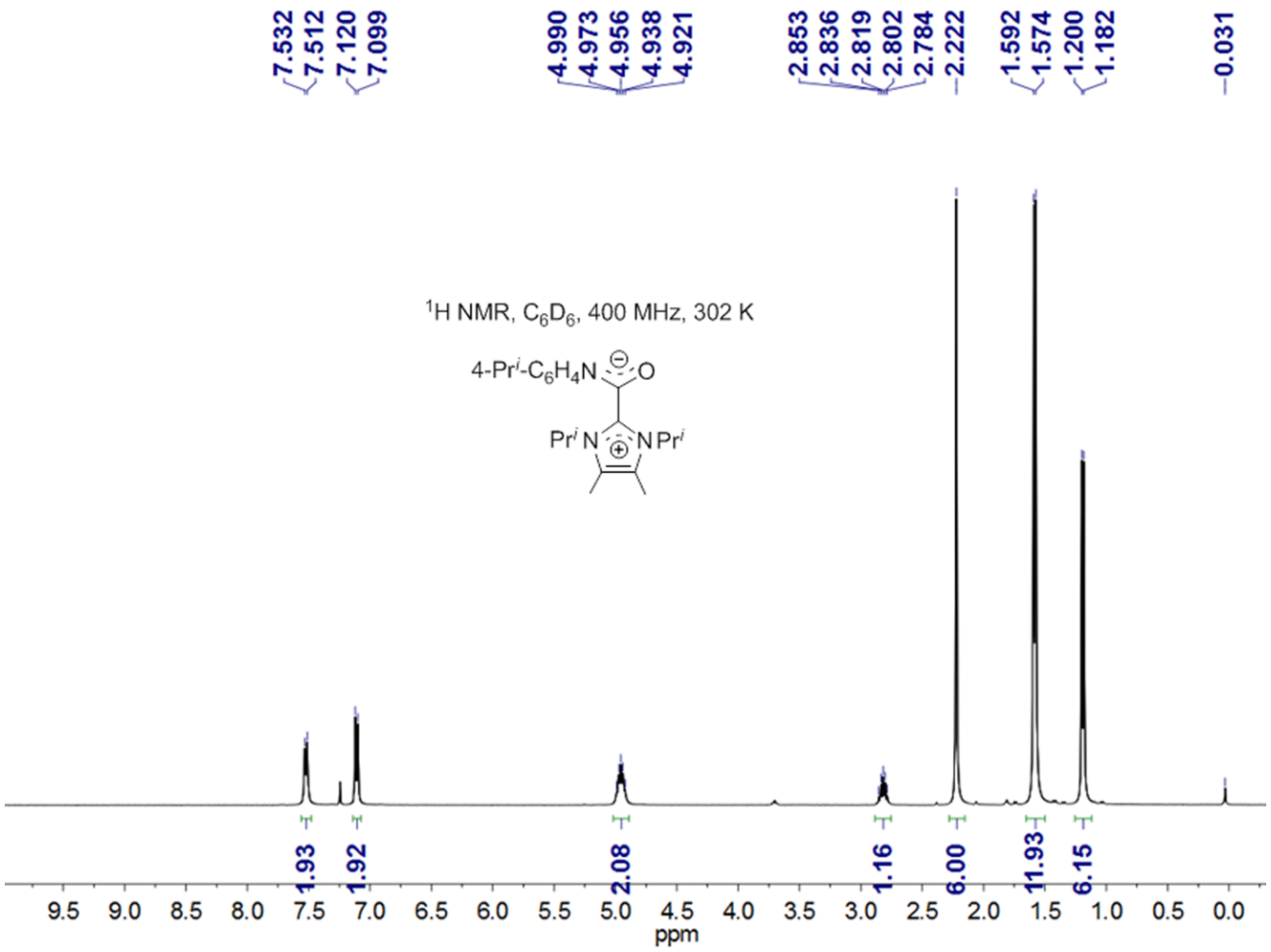

Figure S16. ^{1}H NMR spectrum of **6** in C_6D_6.

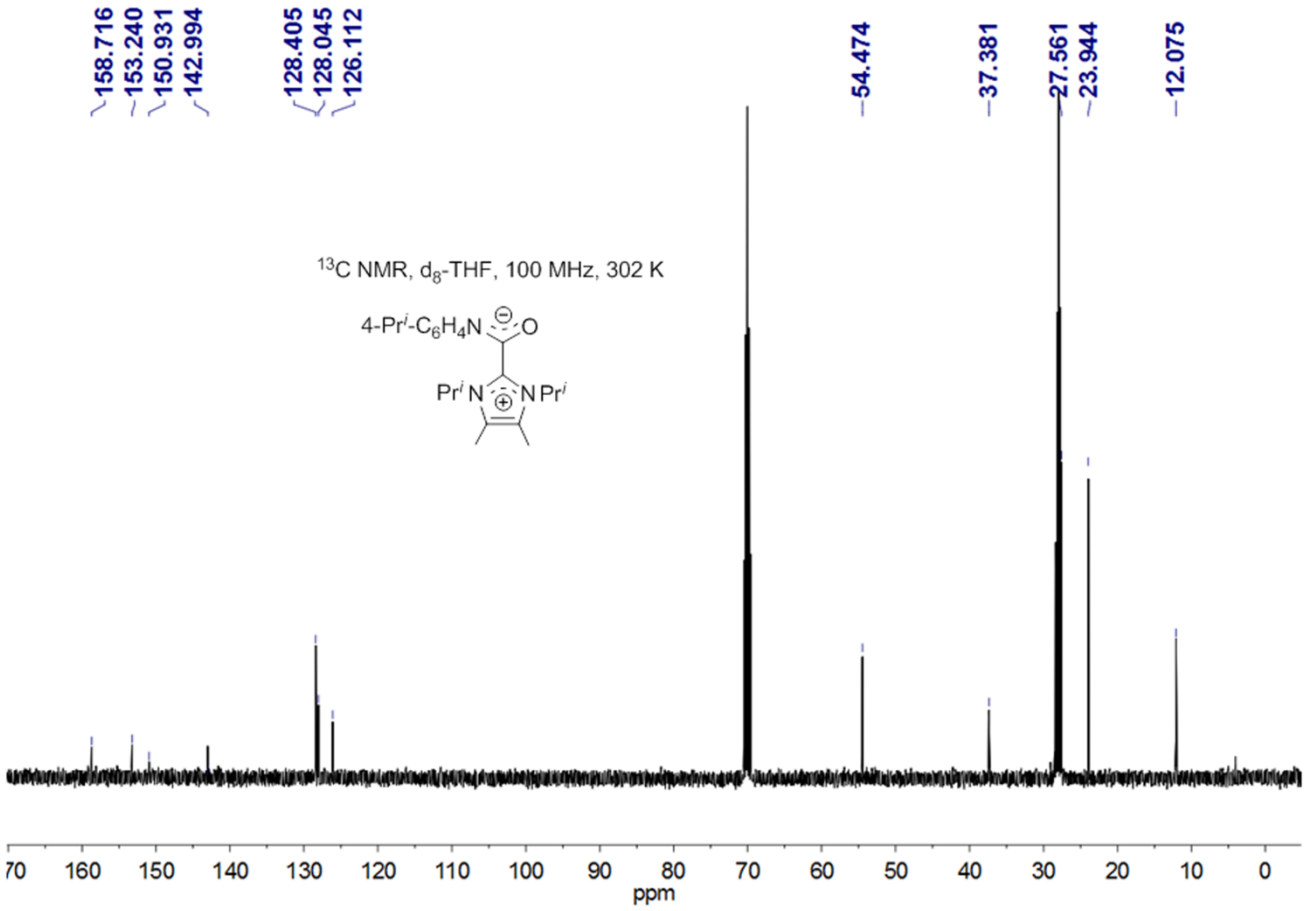

Figure S17. ^{13}C NMR spectrum of **6** in d_8-THF.

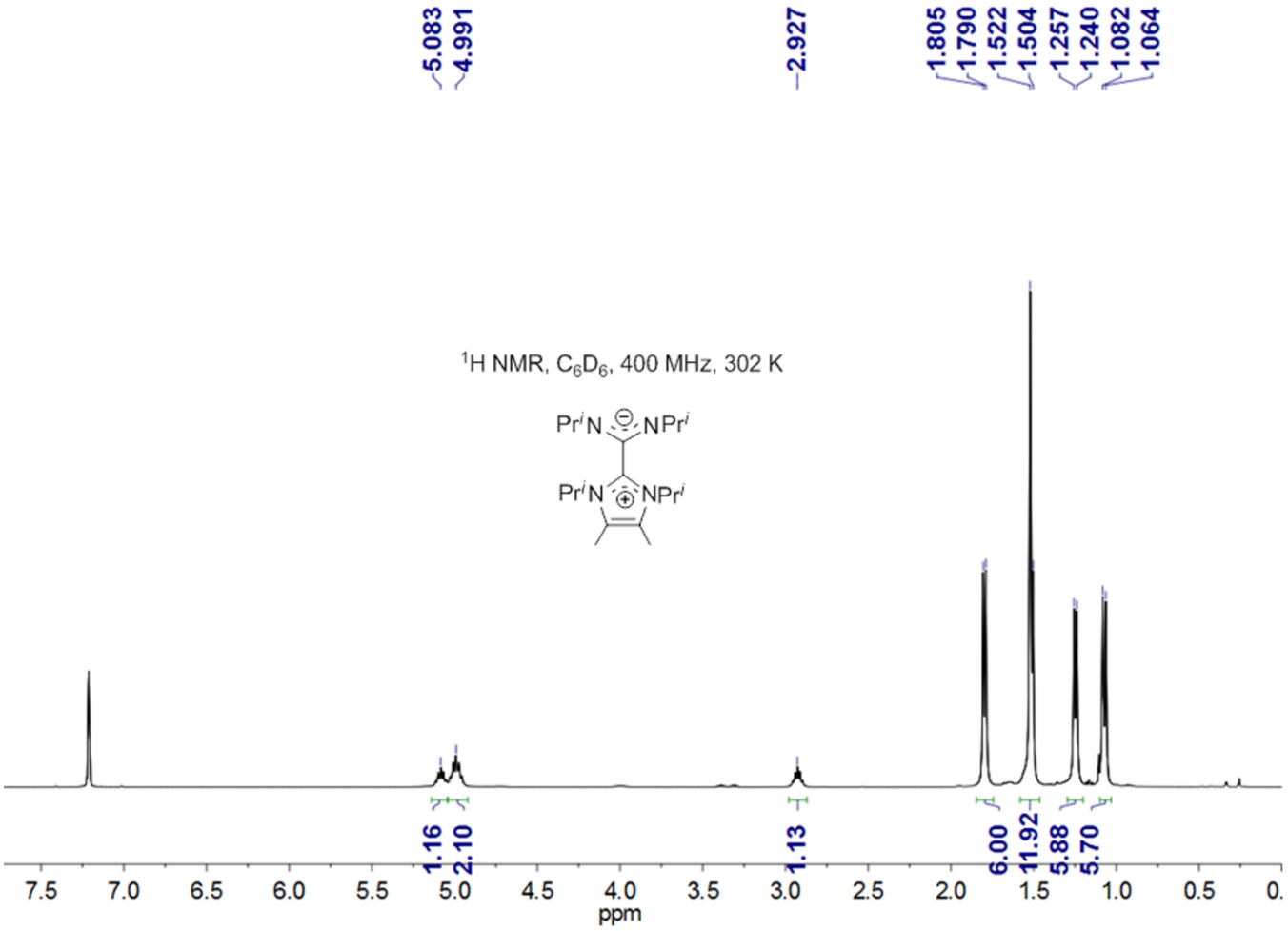

Figure S18. ^{1}H NMR spectrum of **7** in C_6D_6.

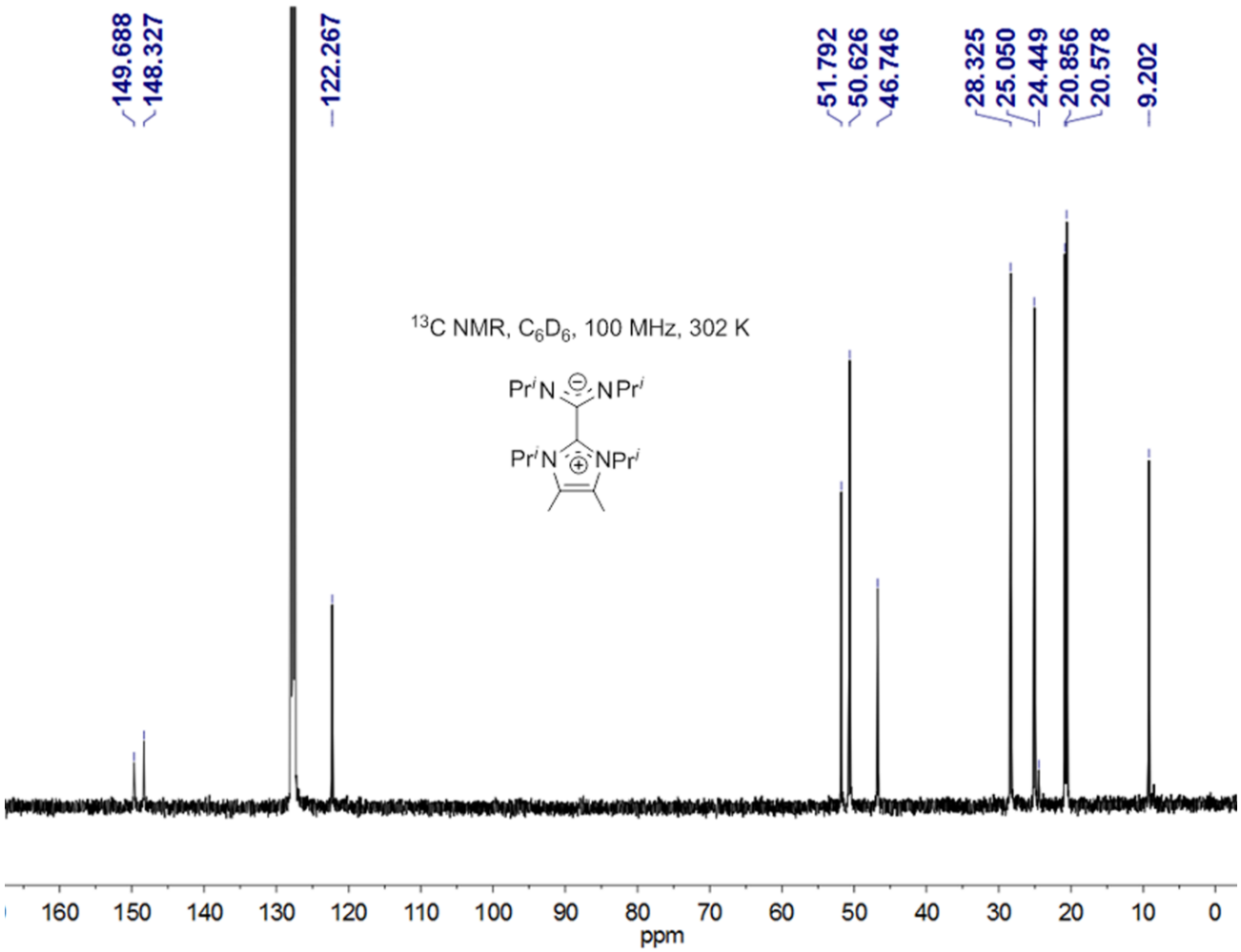

Figure S19. ^{13}C NMR spectrum of **7** in C_6D_6.

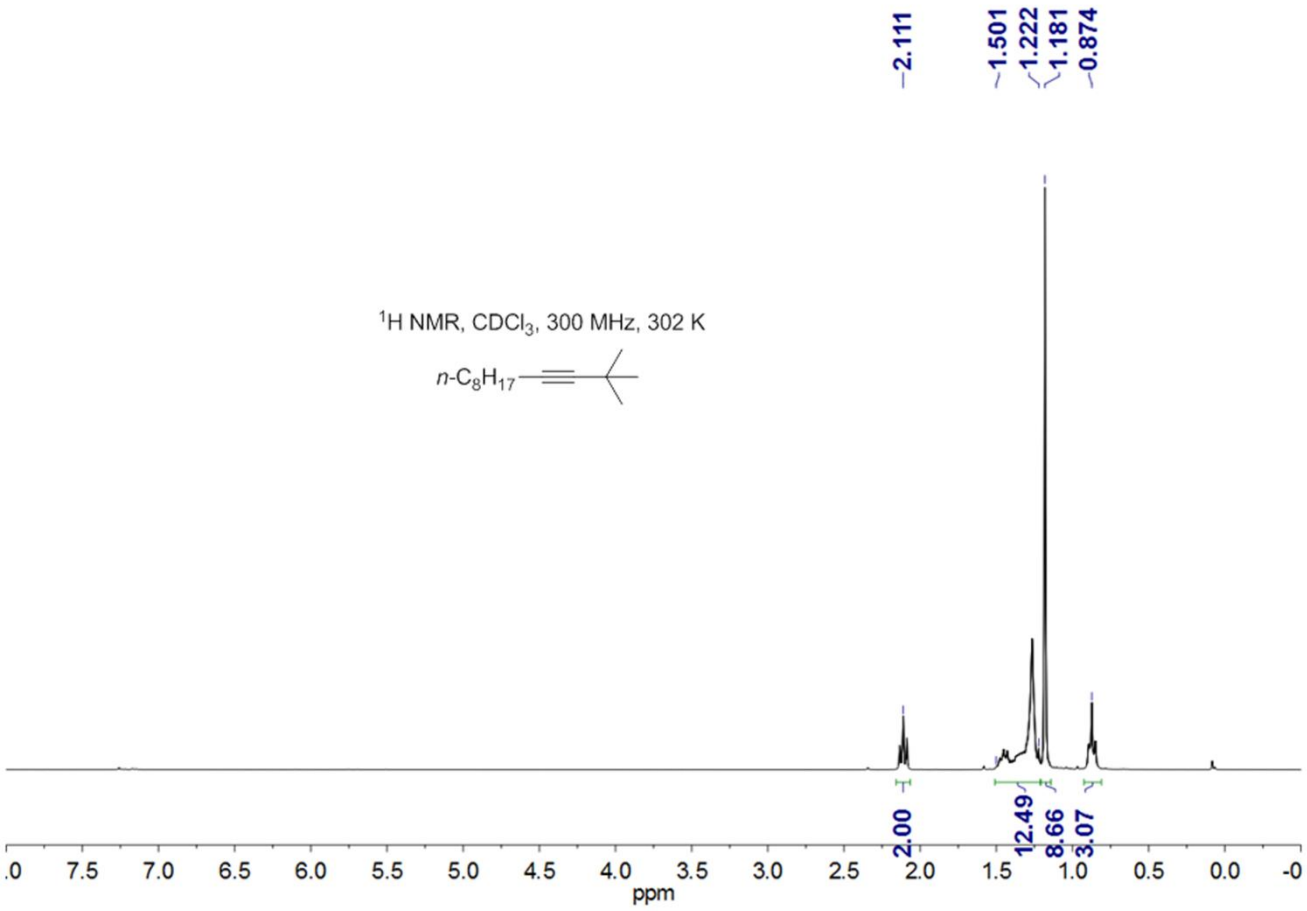

Figure S20. ^{1}H NMR spectrum of n-C_8H_{17}-C≡CBu^t in $CDCl_3$.

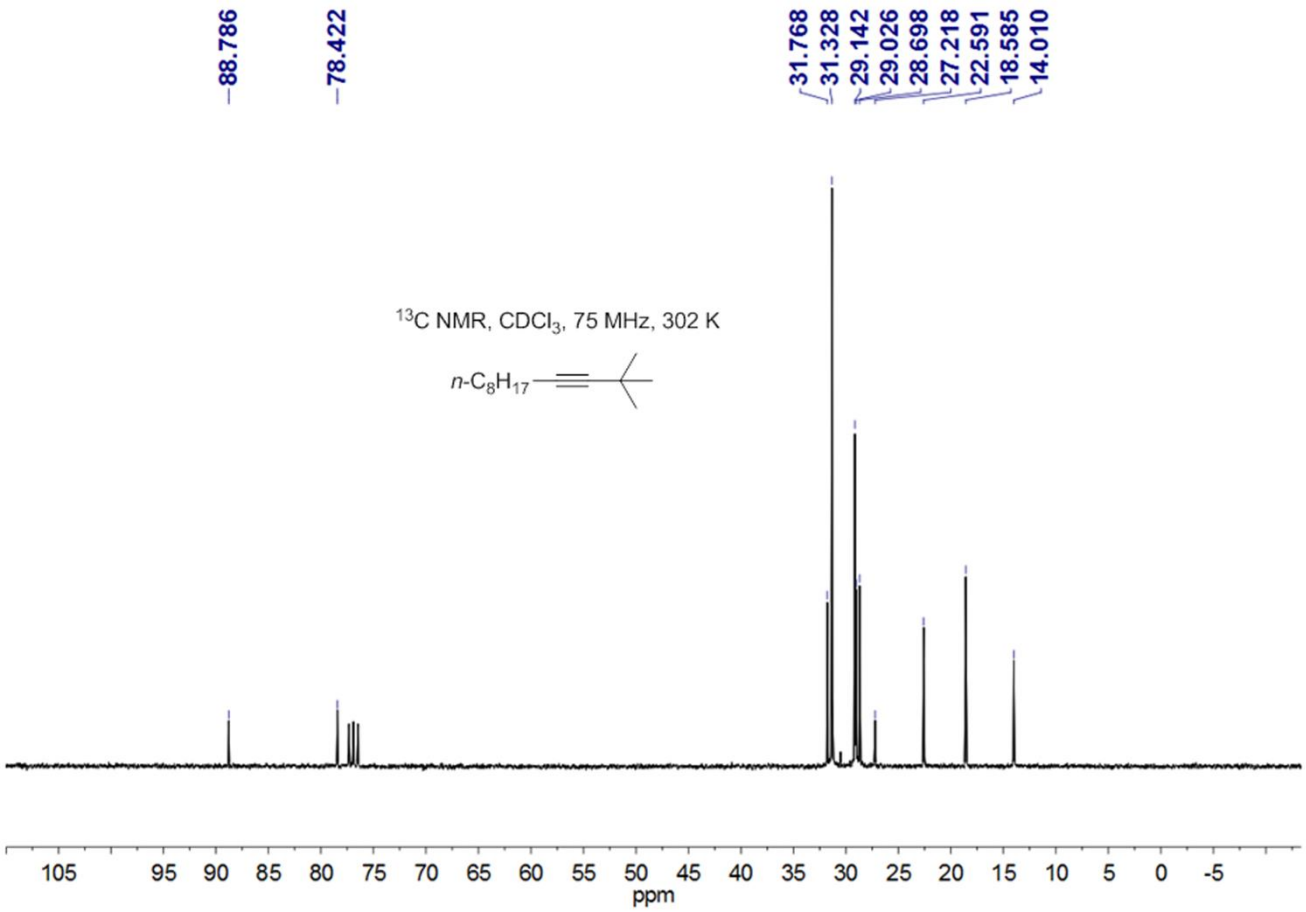

Figure S21. ^{13}C NMR spectrum of *n*-C_8H_{17}-C≡CBu^t in $CDCl_3$.

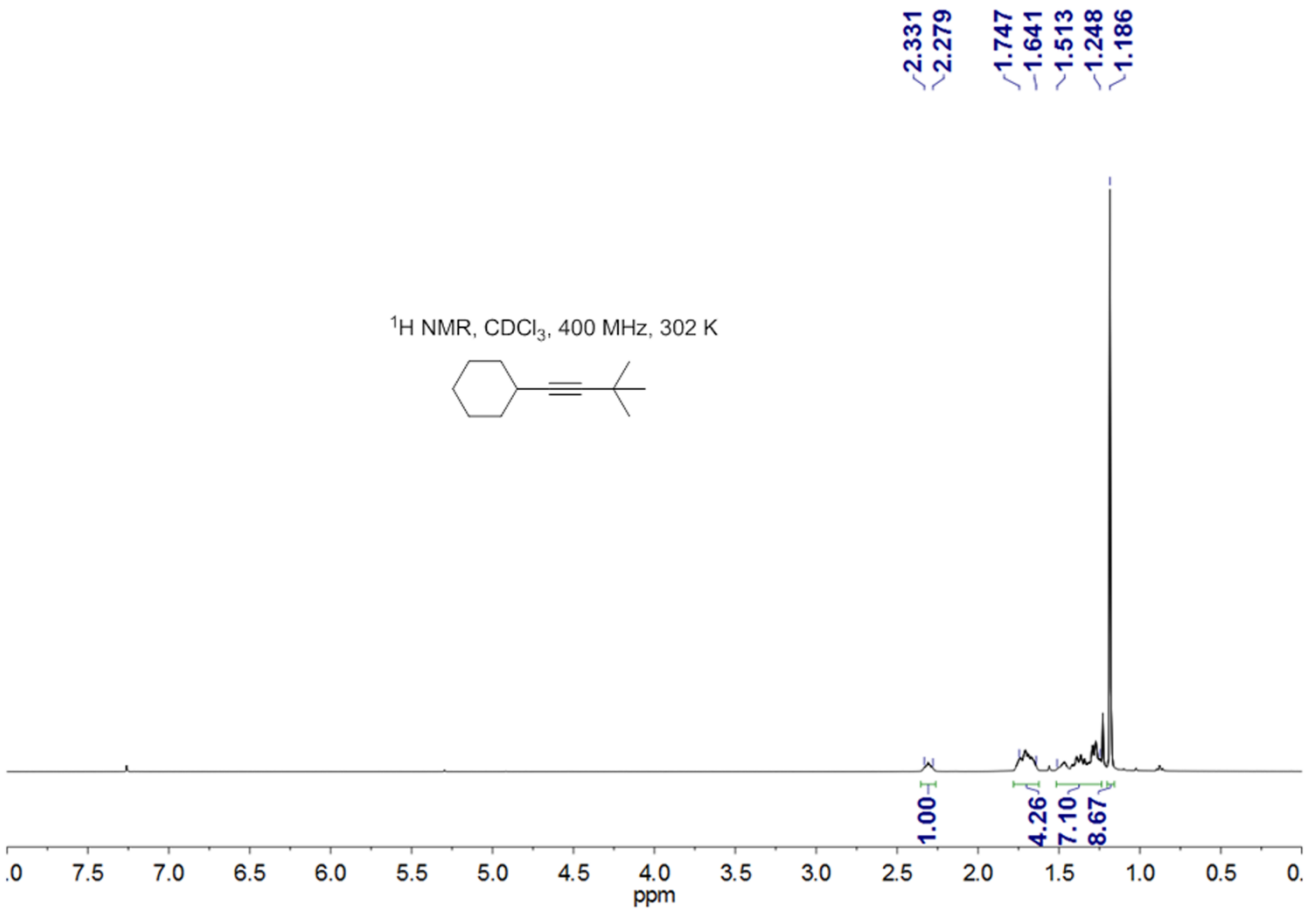

Figure S22. ^{1}H NMR spectrum of *c*-C_6H_{11}-C≡CBu^t in $CDCl_3$.

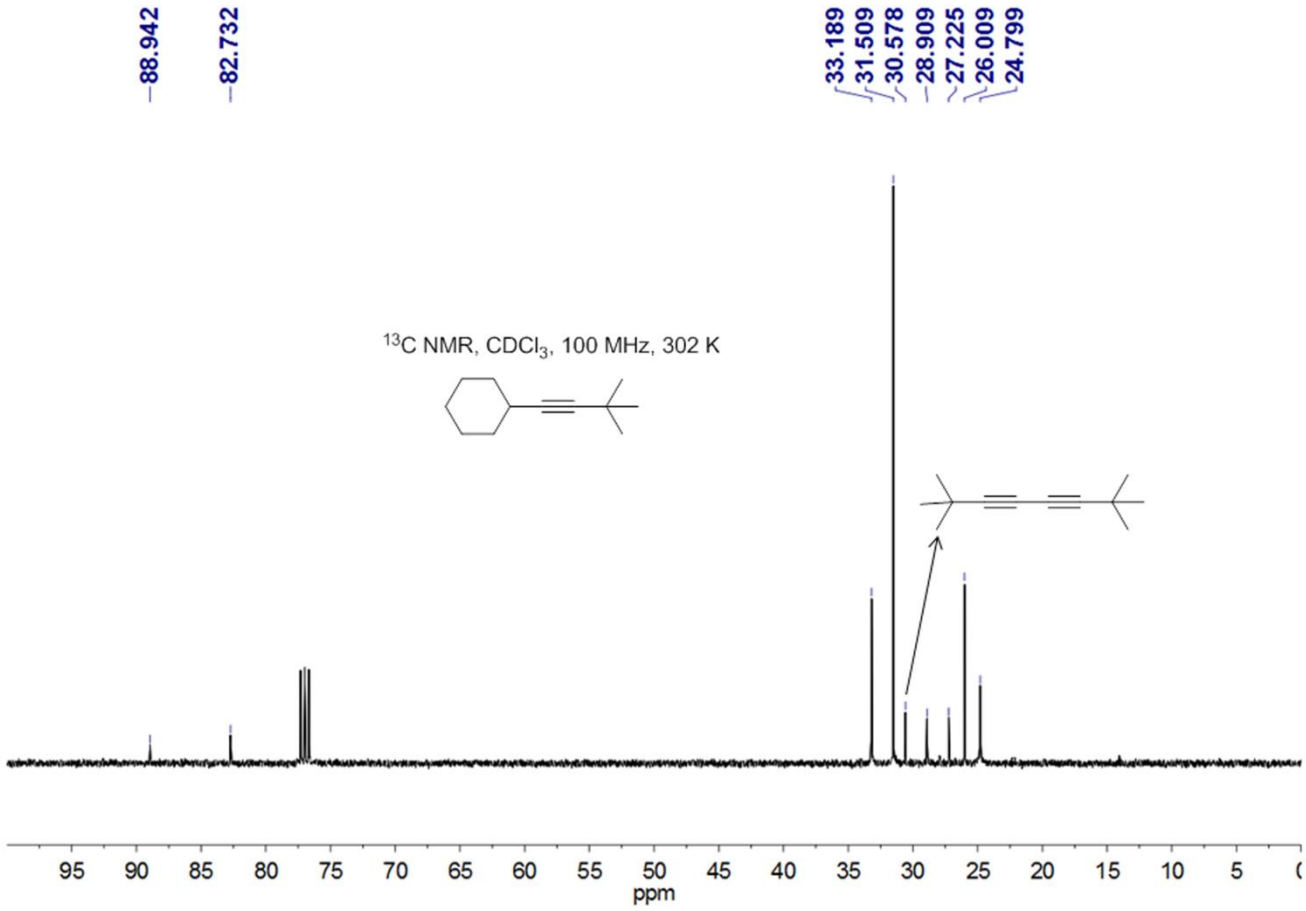

Figure S23. ^{13}C NMR spectrum of *c*-C_6H_{11}-C≡CBu^t in $CDCl_3$.

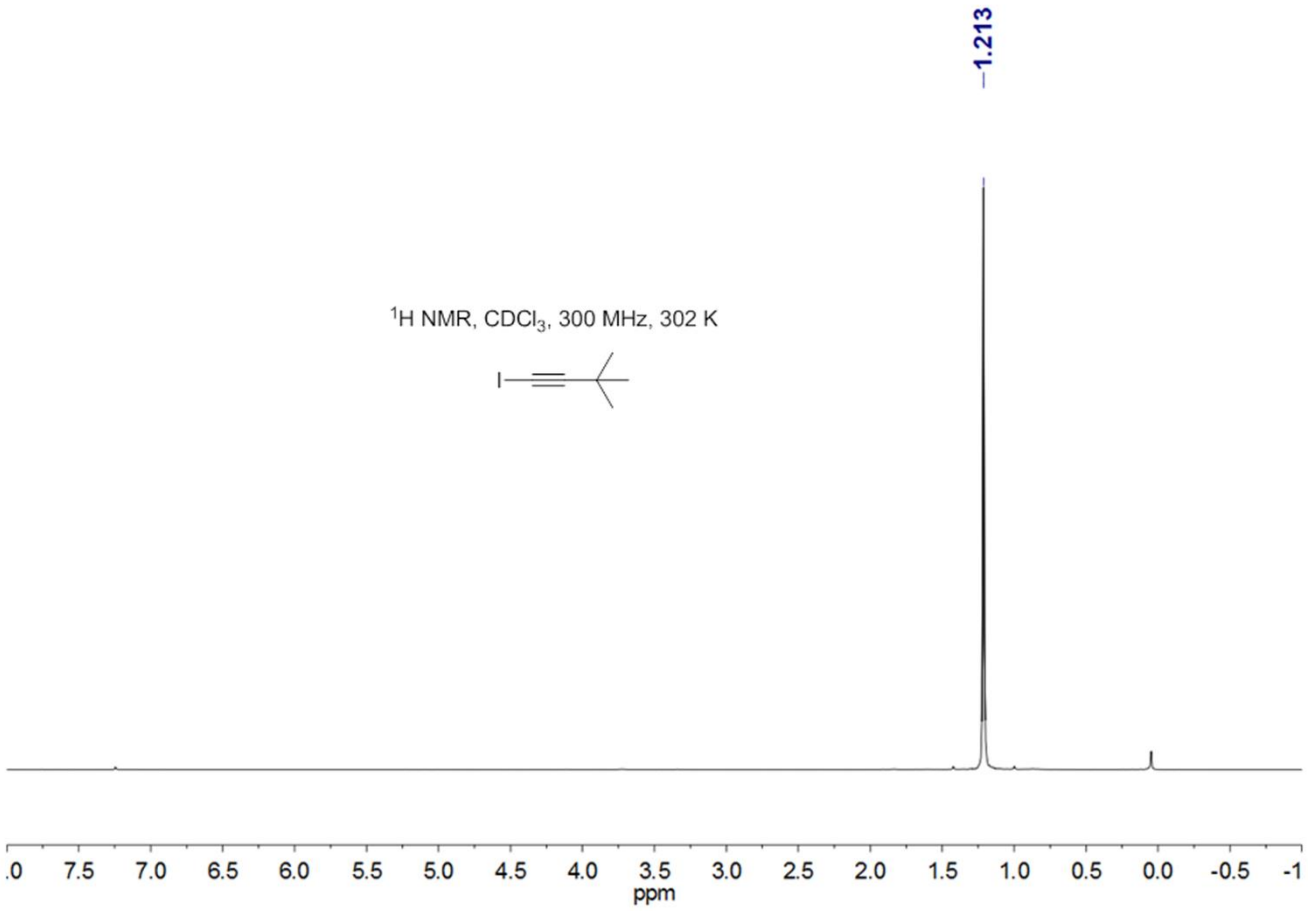

Figure S24. ^{1}H NMR spectrum of Bu^{t}C≡C-I in $CDCl_3$.

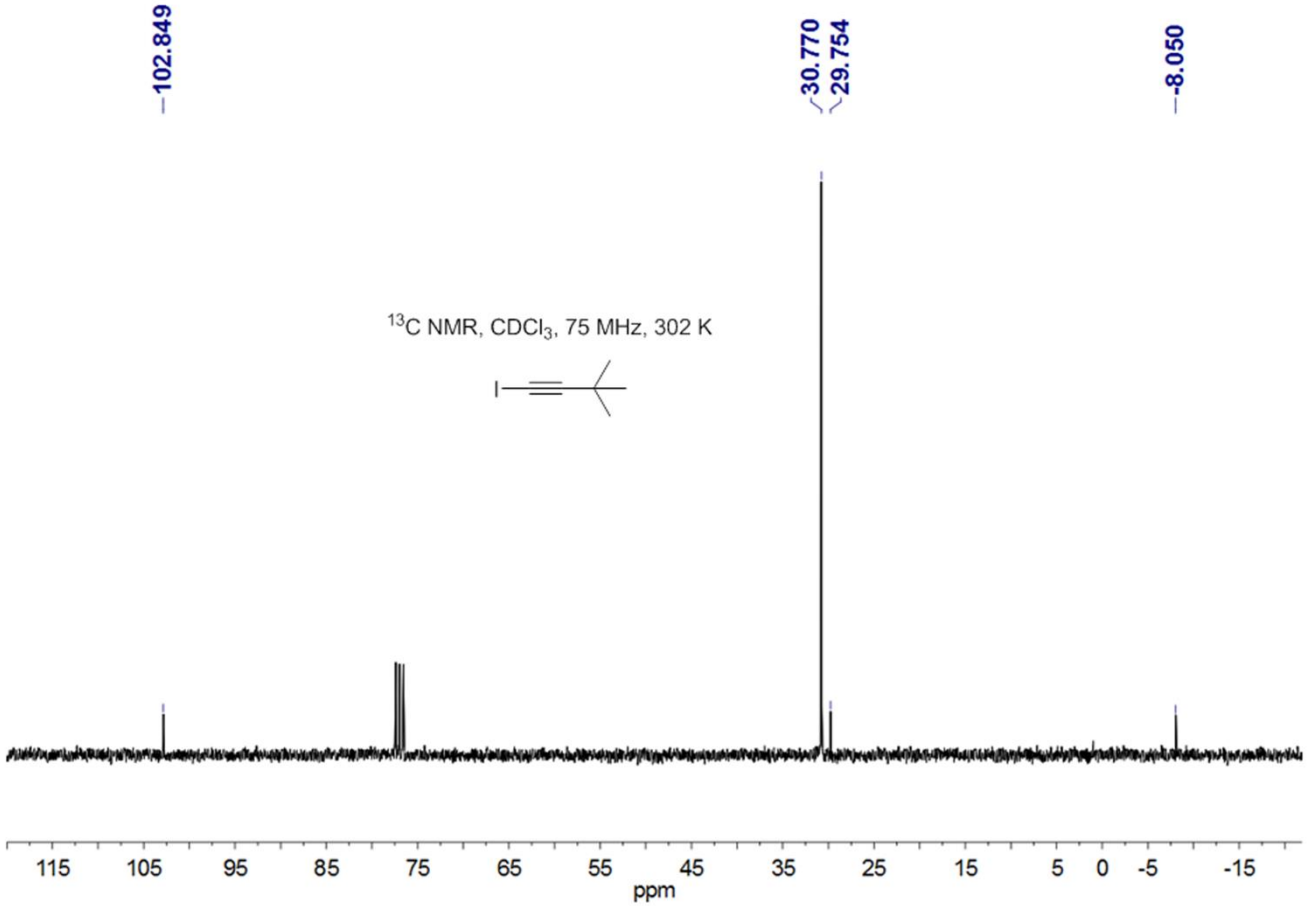

Figure S25. ^{13}C NMR spectrum of Bu^{t}C≡C-I in $CDCl_3$.

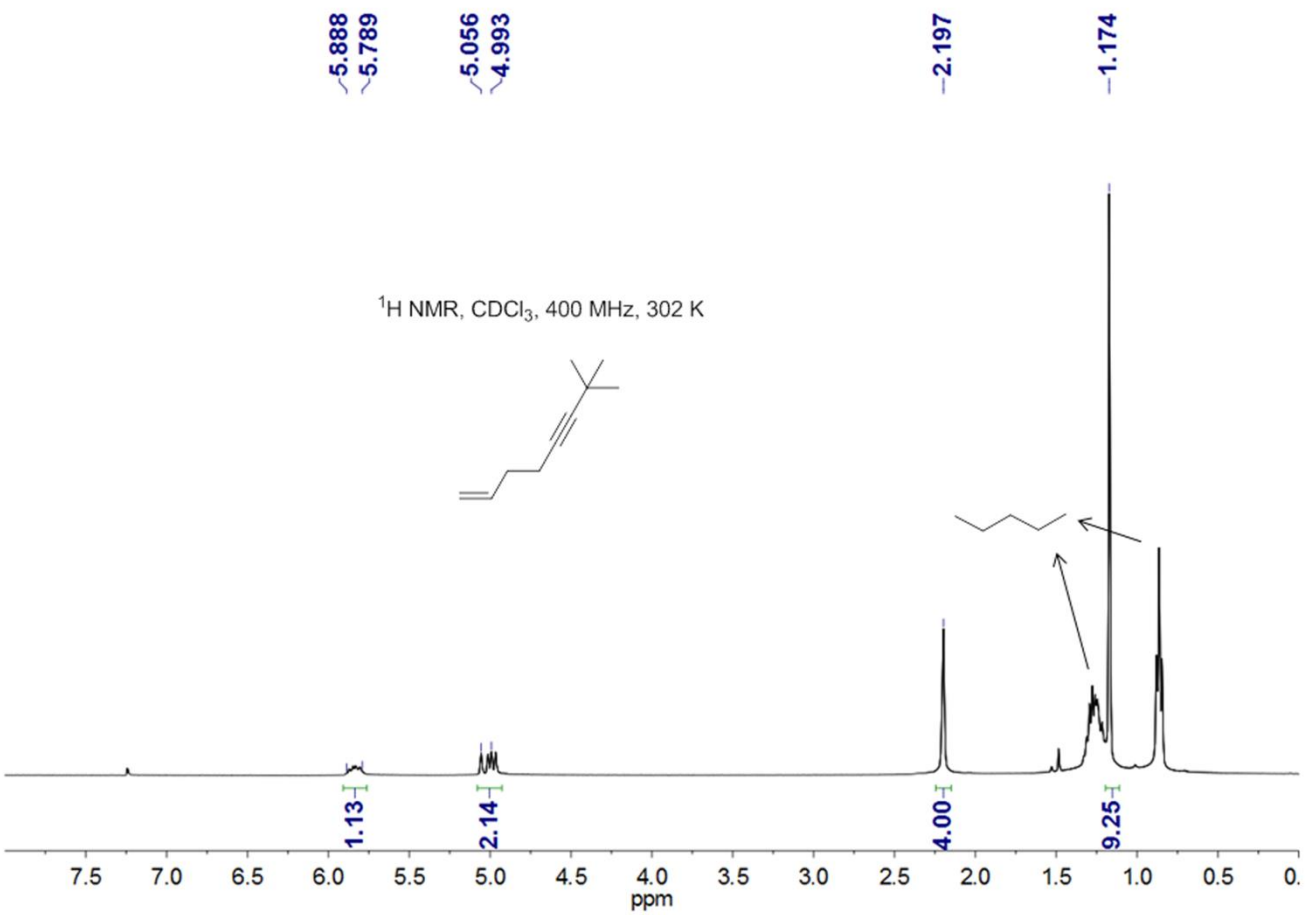

Figure S26. ^{1}H NMR spectrum of CH_2=CH$(CH_2)_2$C≡CBu^t in $CDCl_3$.

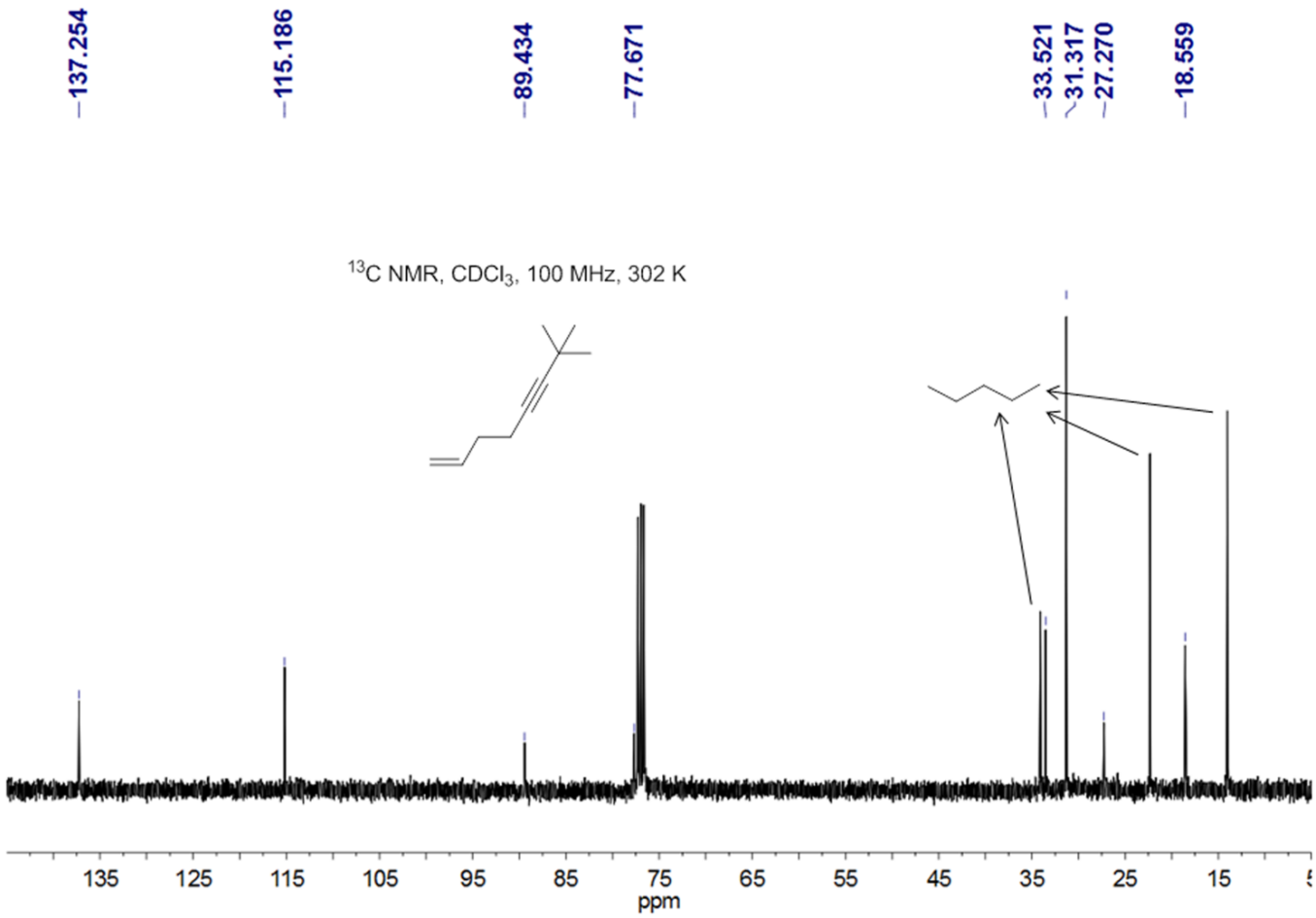

Figure S27. ^{13}C NMR spectrum of $CH_2{=}CH(CH_2)_2C{\equiv}CBu^t$ in $CDCl_3$.

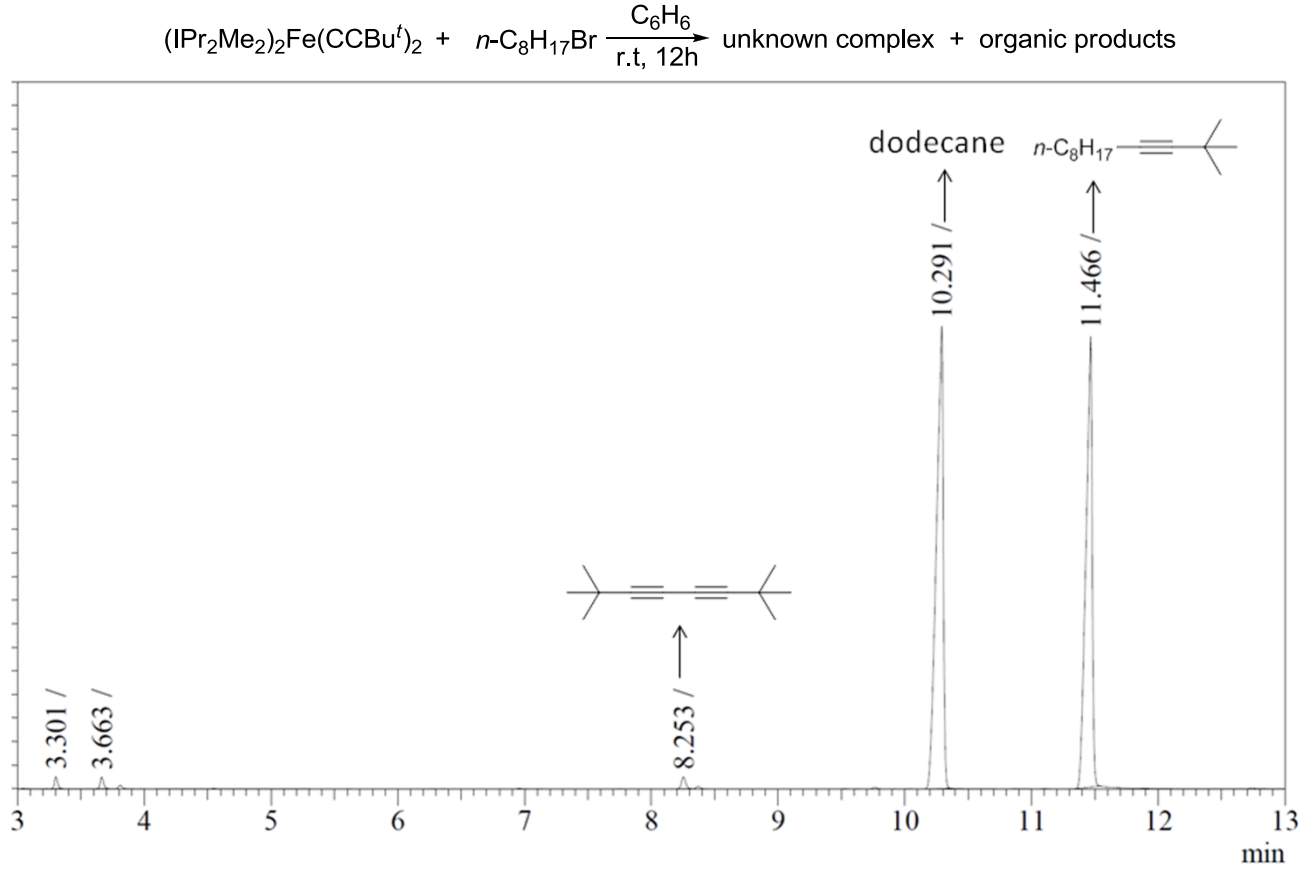

Figure S28. The GC graph for the quenched reaction mixture of **1** with *n*-$C_8H_{17}Br$.

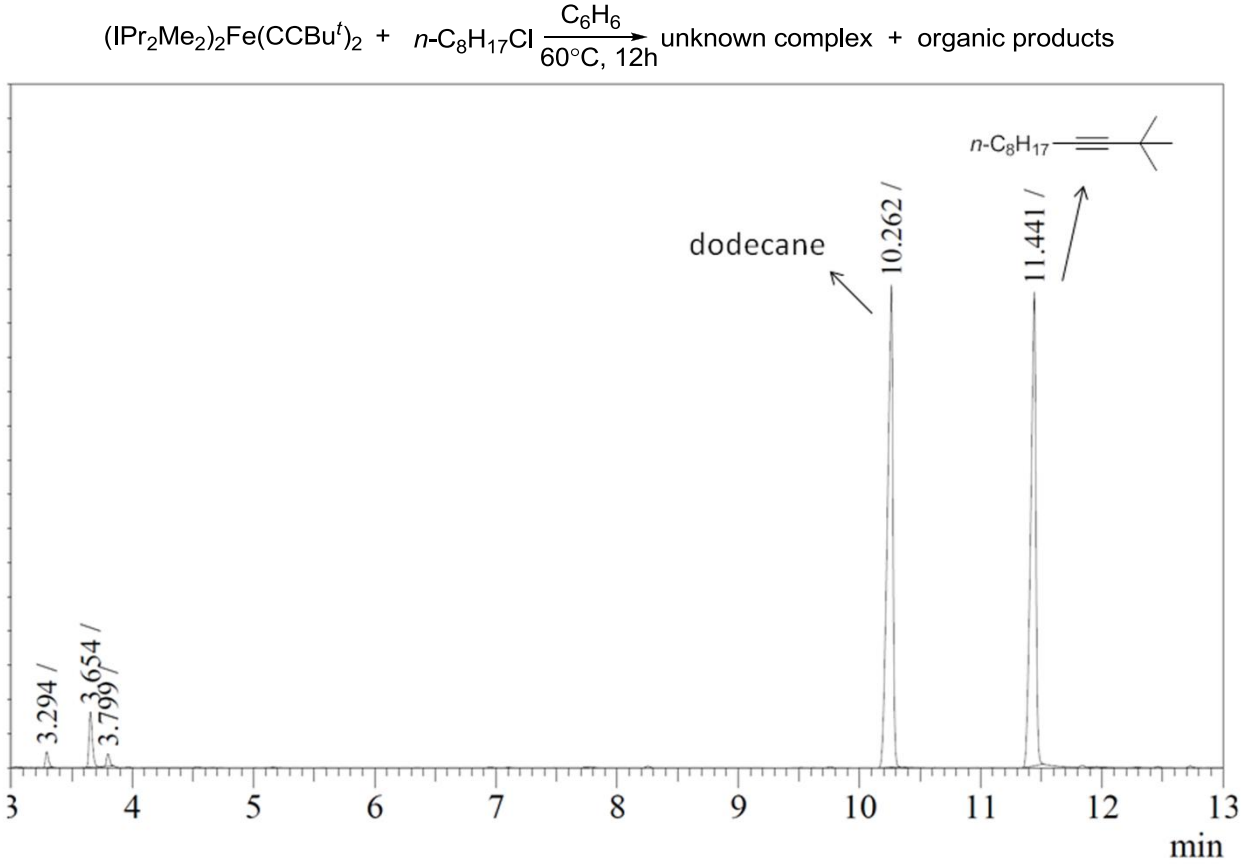

Figure S29. The GC graph for the quenched reaction mixture of **1** with *n*-$C_8H_{17}Cl$.

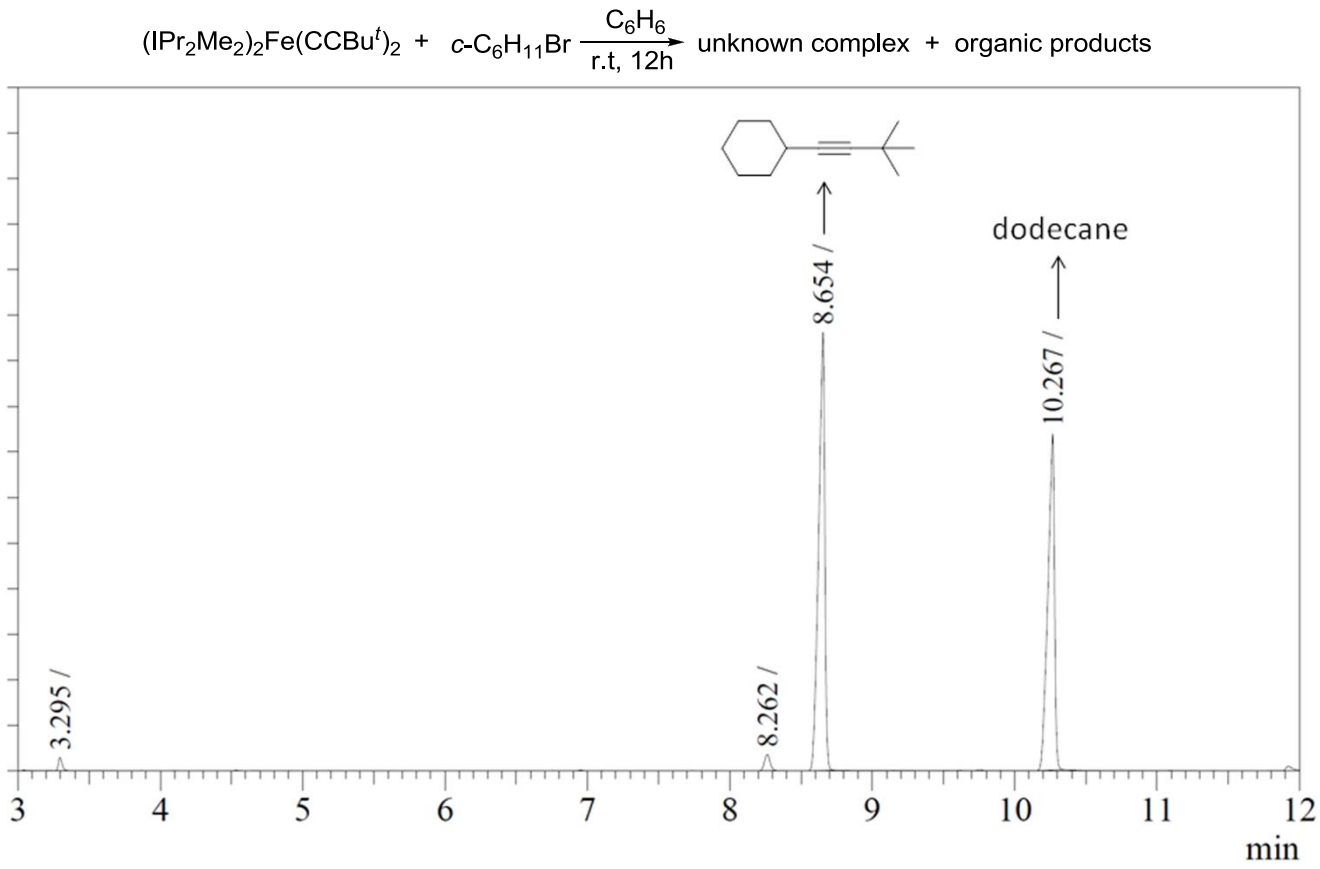

Figure S30. The GC graph for the quenched reaction mixture of **1** with *c*-$C_6H_{11}Br$.

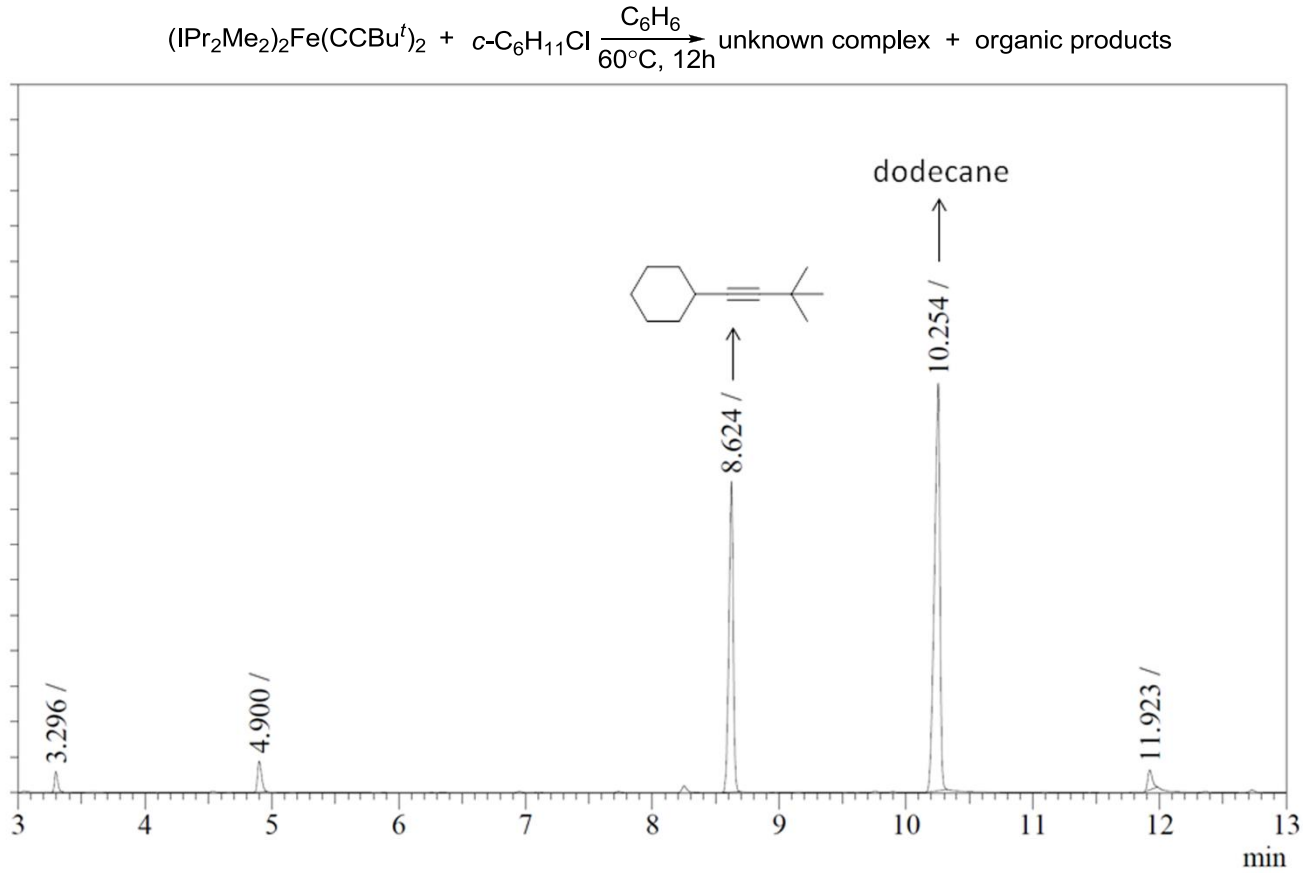

Figure S31. The GC graph for the quenched reaction mixture of **1** with *c*-$C_6H_{11}Cl$.

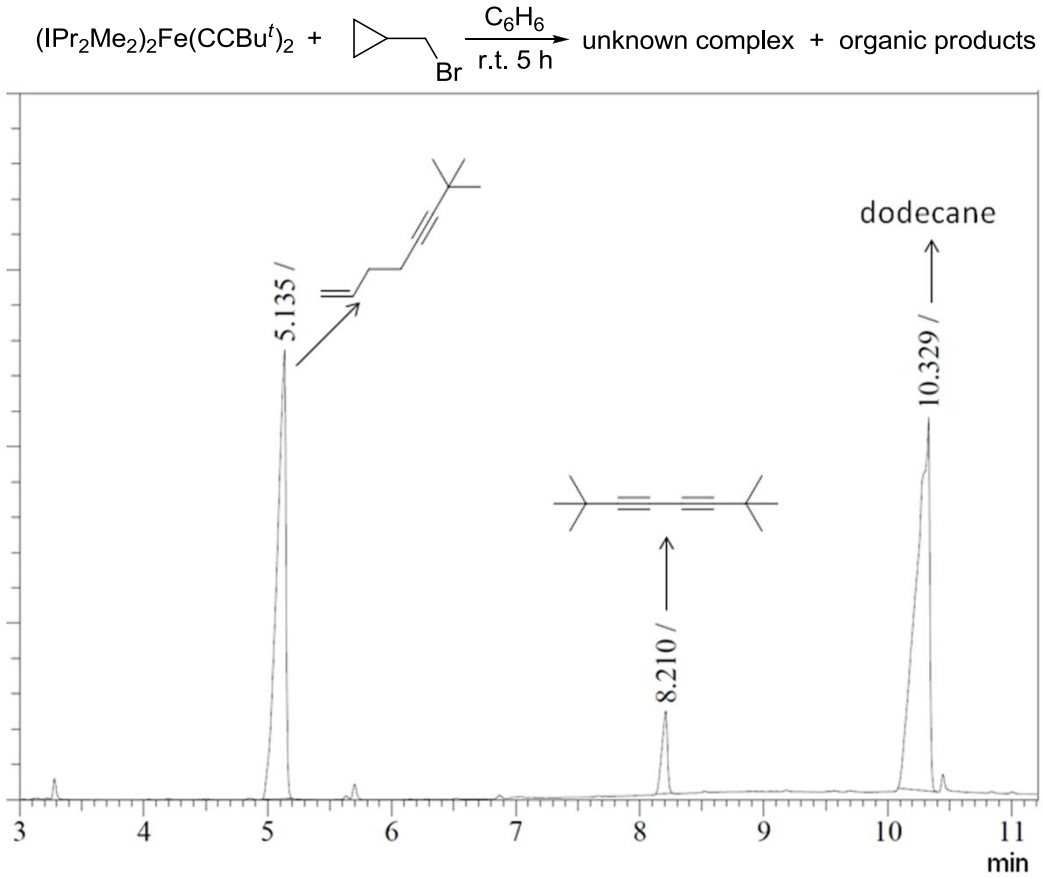

Figure S32. The GC graph for the quenched reaction mixture of **1** with *c*-$C_3H_5CH_2Br$.

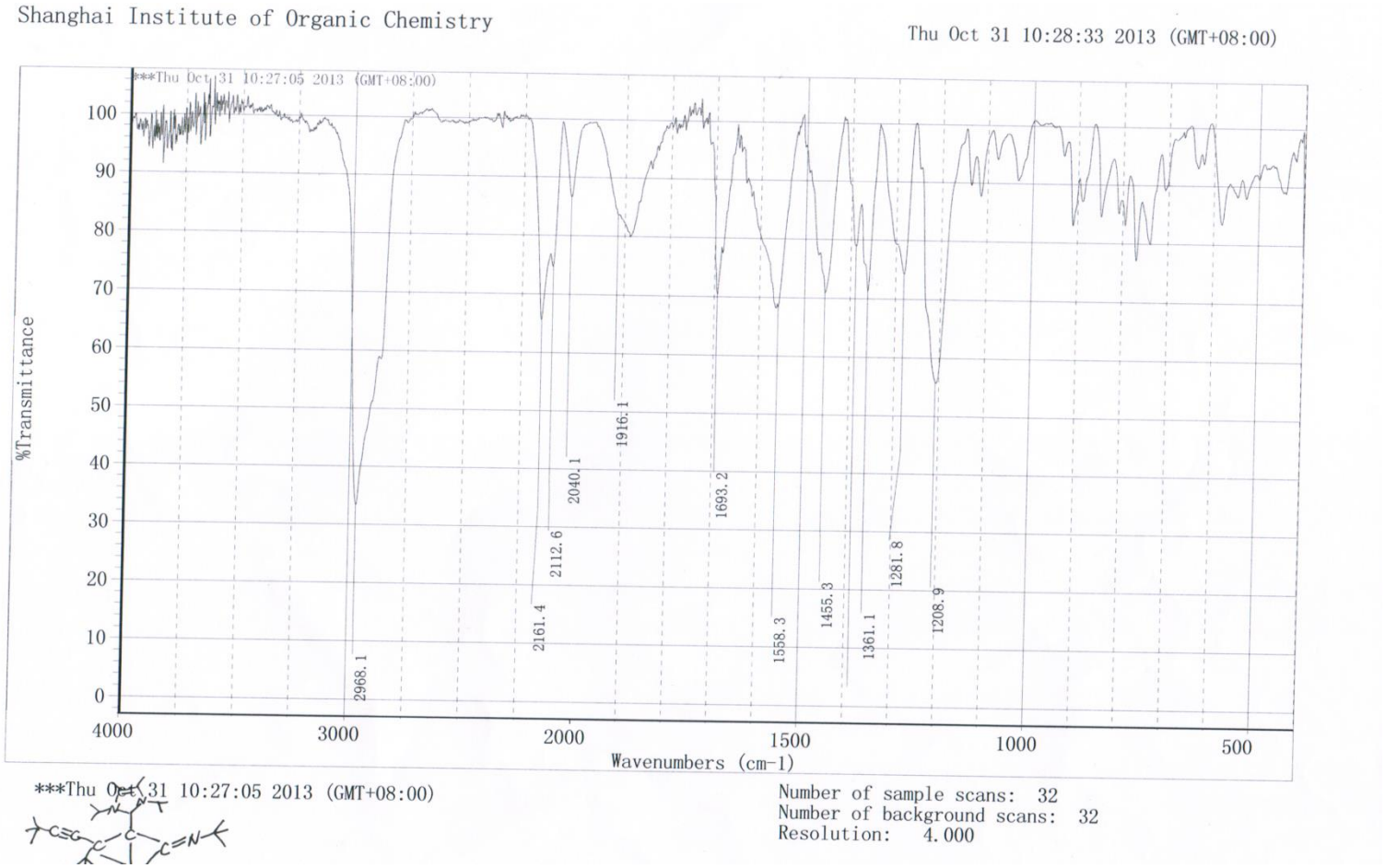

Figure S33. The IR spectrum of [η^3-{(Bu^tCC)(Bu^t)CC(IPr_2Me_2)C(NBu^t)}Fe($NCBu^t$)$_3$] (**5**)